Chemical Engineering Science 64 (2009) 3159–3178

Contents lists available at ScienceDirect

Chemical Engineering Science

journal homepage: www.elsevier.com/locate/ces

Unified Maxwell–Stefan description of binary mixture diffusion in *micro*- and *meso*-porous materials

R. Krishna*, J.M. van Baten

Van 't Hoff Institute for Molecular Sciences, University of Amsterdam, Nieuwe Achtergracht 166, 1018 WV Amsterdam, The Netherlands

ARTICLE INFO

Article history:
Received 26 January 2009
Received in revised form 23 March 2009
Accepted 26 March 2009
Available online 7 April 2009

Keywords:
Zeolites
Metal–organic frameworks
Exchange coefficient
Maxwell–Stefan
Diffusion
Binary mixture
Correlation effects

ABSTRACT

The Maxwell–Stefan (M–S) formulation for binary mixture diffusion in *micro*-porous materials such as zeolites, metal organic frameworks (MOFs), and covalent organic frameworks (COFs), that have pore sizes typically smaller than 2 nm, is formulated in a manner that is consistent with corresponding description for *meso*-porous systems. The M–S equations are set up in terms of species concentrations, c_i, defined in terms of accessible pore volume space. Molecular dynamics simulations were carried out to determine the exchange coefficients $Đ_{12}$ for a large variety of binary mixtures in zeolites (MFI, AFI, BEA, FAU, LTA, CHA, and DDR), MOFs (CuBTC, IRMOF-1, Zn(bdc)dabco, Co(bdc)dabco, MIL-47, Co-FA, Mn-FA, and Zn(tbip)), COFs (COF-102, COF-103, and COF-108), and cylindrical silica pores of varying diameters. The exchange coefficients $Đ_{12}$ in all structures were found to be related by a constant factor, F, with the corresponding M–S diffusivity for binary *fluid* mixture, $Đ_{12,fl}$, at the same total mixture concentration, c_t, as within the pores. The factor F is primarily dictated by the degree of confinement of the guest molecules within the channels, defined as the ratio of the characteristic sizes of the guest molecules to that of the host channels. For *meso*-porous cylindrical silica pores: $F = 1$, and $Đ_{12} = Đ_{12,fl}$. For CuBTC, MIL-47, IRMOF-1, and COFs, that have structures with a high fractional open space and channel dimensions of 0.8–1.85 nm, the factor F is found to be in the range 0.55–0.85. For structures such as MFI, BEA, Co-FA, Mn-FA, and Zn(tbip) that have smaller fractional open space, and channels smaller than 0.6 nm, the factor F has values < 0.2. The major conclusion of this study is that fluid mixture diffusivity $Đ_{12,fl}$ provides a good starting point for an engineering estimate of the exchange coefficient $Đ_{12}$ in porous materials.

1. Introduction

In the development and design of separation and reaction equipment involving *micro*- and *meso*-porous materials, the proper description of mixture diffusion is of vital importance (Delgado and Rodrigues, 2001; Farooq and Ruthven, 1991; Gavalas, 2008; Hansen et al., 2009; Higgins et al., 2009; Kärger and Ruthven, 1992; Keskin et al., 2009; Ruthven, 1984; van de Graaf et al., 1999; Wang et al., 1999; Wang and LeVan, 2007, 2008). In the published literature the models for diffusion in these materials have adopted two distinctly different approaches, the need for which can be appreciated by considering the Lennard-Jones interaction potential (normalized with respect to the energy parameter, ε) for methane and a silica pore wall; see Fig. 1a. The minimum in the potential energy for interaction with the wall surface occurs at a distance 0.39 nm from the wall, and for distances greater than about 0.6 nm from the pore wall the interaction potential is virtually zero. In *meso*-porous materials such as MCM-41, SBA-16, and Vycor glass that have pore sizes in the range 2–50 nm, there is a central core region where the influence of interactions of the molecules with the pore wall is either small or negligible. As illustration, Fig. 1b shows the radial distribution of the loading of methane as a function of the distance from the wall of a 3 nm pore; the core region is demarcated. The maximum in the concentration distribution occurs at the position corresponding to the minimum in the Lennard-Jones interaction potential. Meso-pore diffusion is governed by a combination of molecule–molecule and molecule–pore wall interactions. The Maxwell–Stefan (M–S) equations are commonly written for mixture diffusion as (Kerkhof, 1996; Krishna and van Baten, 2009a; Young and Todd, 2005)

$$-\frac{c_i}{RT}\nabla\mu_i = \sum_{\substack{j=1\\ j\neq i}}^{n}\frac{x_jN_i - x_iN_j}{Đ_{ij}} + \frac{N_i}{Đ_i}; \quad i = 1,2,\ldots,n \tag{1}$$

In Eq. (1) $Đ_i$ is the M–S diffusivities of species i, portraying the interaction between component i in the mixture with the surface, or wall, of the pore; it reflects a conglomerate of Knudsen and surface

* Corresponding author. Tel.: +31 20 257007; fax: +31 20 5255604.
E-mail address: r.krishna@uva.nl (R. Krishna).

0009-2509/$ - see front matter © 2009 Elsevier Ltd. All rights reserved.
doi:10.1016/j.ces.2009.03.047

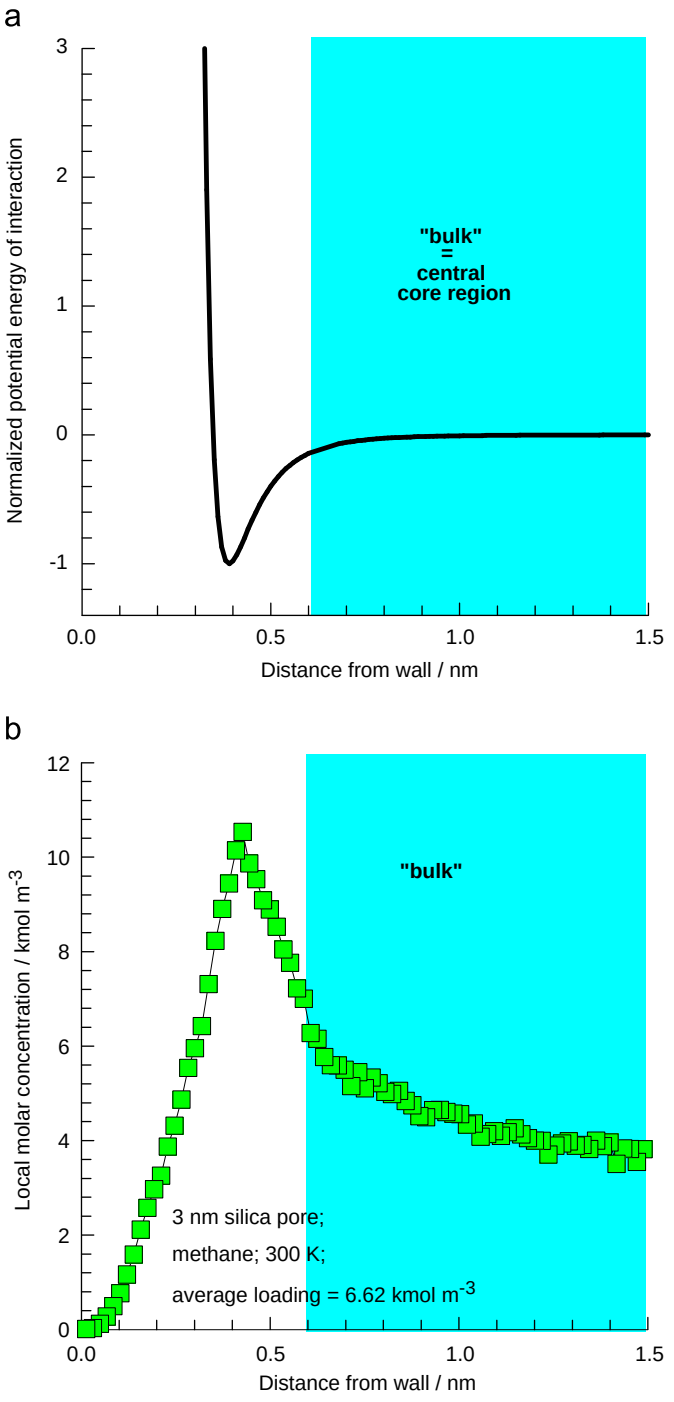

Fig. 1. (a) Normalized Lennard-Jones interaction potential for methane and O atoms in a silica wall surface. (b) Radial distribution of methane in a 3 nm cylindrical silica pore in which the average loading $c_i = 6.62\,\text{kmol m}^{-3}$. The distribution was obtained from a CBMC simulation of adsorption.

diffusion, along with the viscous flow contribution. It is noteworthy that Eq. (1) do not correspond to the dusty gas model (Mason and Malinauskas, 1983), that been a subject of intense criticism in the recent literature due to some inconsistencies and handling of the viscous flow contribution (Kerkhof, 1996; Young and Todd, 2005). The $Đ_{ij}$ are exchange coefficients representing interaction between components i with component j. The Onsager reciprocal relations prescribe

$$Đ_{ij} = Đ_{ji} \tag{2}$$

The c_i are the molar concentrations defined in terms of the pore volume, and the x_i represent the component mole fractions

$$x_i = c_i/c_t; \quad i = 1, 2, \ldots, n \tag{3}$$

Molecular dynamics (MD) simulations for diffusion of a wide variety of binary ($n = 2$) mixtures in cylindrical meso-pores of silica with various diameters have shown that the $Đ_{12}$ can be identified with the *fluid* phase diffusivity, $Đ_{12,fl}$, in the binary mixture at the same total molar loadings c_t as within the pore (Krishna and van Baten, 2009a). The $Đ_i$ have the same values as for the *pure* component diffusion, evaluated at the total loading in the mixture, c_t. These are very convenient results, and allow mixture diffusion characteristics to be estimated for engineering purposes from: (1) unary diffusion data within the same pore and (2) *fluid* phase mixture diffusivity at same loading c_t.

In *micro*-porous materials such as zeolites, metal organic frameworks (MOFs), and covalent organic frameworks (COFs), that have typically pore sizes in the 0.35–2 nm range, the description of diffusion is significantly more complicated than within meso-pores. Within micro-pores the guest molecules are always within the influence of the force field exerted with the wall and we have to reckon with the motion of *adsorbed* molecules, and there is no "bulk" fluid region. In the published literature, the M–S equations for binary mixture diffusion in zeolites and MOFs are set up in a different manner (Chempath et al., 2004; Krishna and van Baten, 2008a,b; Skoulidas et al., 2003)

$$-\frac{\theta_i}{RT}\nabla\mu_i = \sum_{\substack{j=1 \\ j\neq i}}^{n} \frac{c_j N_i - c_i N_j}{c_{i,sat} c_{j,sat} Đ^*_{ij}} + \frac{N_i}{c_{i,sat} Đ_i}; \quad i = 1, 2, \ldots, n \tag{4}$$

with fractional occupancies, θ_i

$$\theta_i \equiv c_i/c_{i,sat}; \quad i = 1, 2, \ldots, n \tag{5}$$

used in place of the component mole fractions x_i. The concentrations c_i are commonly expressed either in terms of moles of component i per m^3 of framework or per kg of framework; in the latter case the left member of Eq. (4) has to be multiplied by the framework density, ρ, in order to yield fluxes N_i in the usual units of $\text{mol m}^{-2}\,\text{s}^{-1}$. The $Đ_i$, defined in Eq. (4), represent molecule–pore wall interactions; there are, however, fundamental differences with the corresponding $Đ_i$, defined in Eq. (1) for meso-porous materials: there is no viscous contribution, and no "Knudsen" character to diffusion mechanism within micro-pores. Eq. (4) have evolved from a description of multicomponent *surface* diffusion (Krishna, 1990). Formally, however, we note that the definition of $Đ_i$ in Eq. (4) is consistent with that in Eq. (1), and there is no need to distinguish between the two sets; this explains the absence of a superscript * on the $Đ_i$ in Eq. (4).

The binary exchange coefficients $Đ^*_{ij}$ defined in Eq. (4) reflect *correlations* in molecular jumps and the Onsager reciprocal relations require that $Đ^*_{ij}$ satisfy

$$c_{j,sat} Đ^*_{ij} = c_{i,sat} Đ^*_{ji}; \quad i,j = 1,2 \tag{6}$$

The estimation of $Đ^*_{ij}$ is the key to the description of mixture diffusion characteristics; this parameter depends on a variety of factors: degree of confinement of the species within the pores, connectivity, and loading. In the published literature the following "empirical" interpolation formula:

$$c_{j,sat} Đ^*_{ij} = [c_{j,sat} Đ^*_{ii}]^{c_i/(c_i+c_j)} [c_{i,sat} Đ^*_{jj}]^{c_i/(c_i+c_j)} = c_{i,sat} Đ^*_{ji} \tag{7}$$

has been recommended for estimating $Đ^*_{ij}$ using information on the *self*-exchange coefficients $Đ^*_{ii}$, obtainable from unary diffusion data

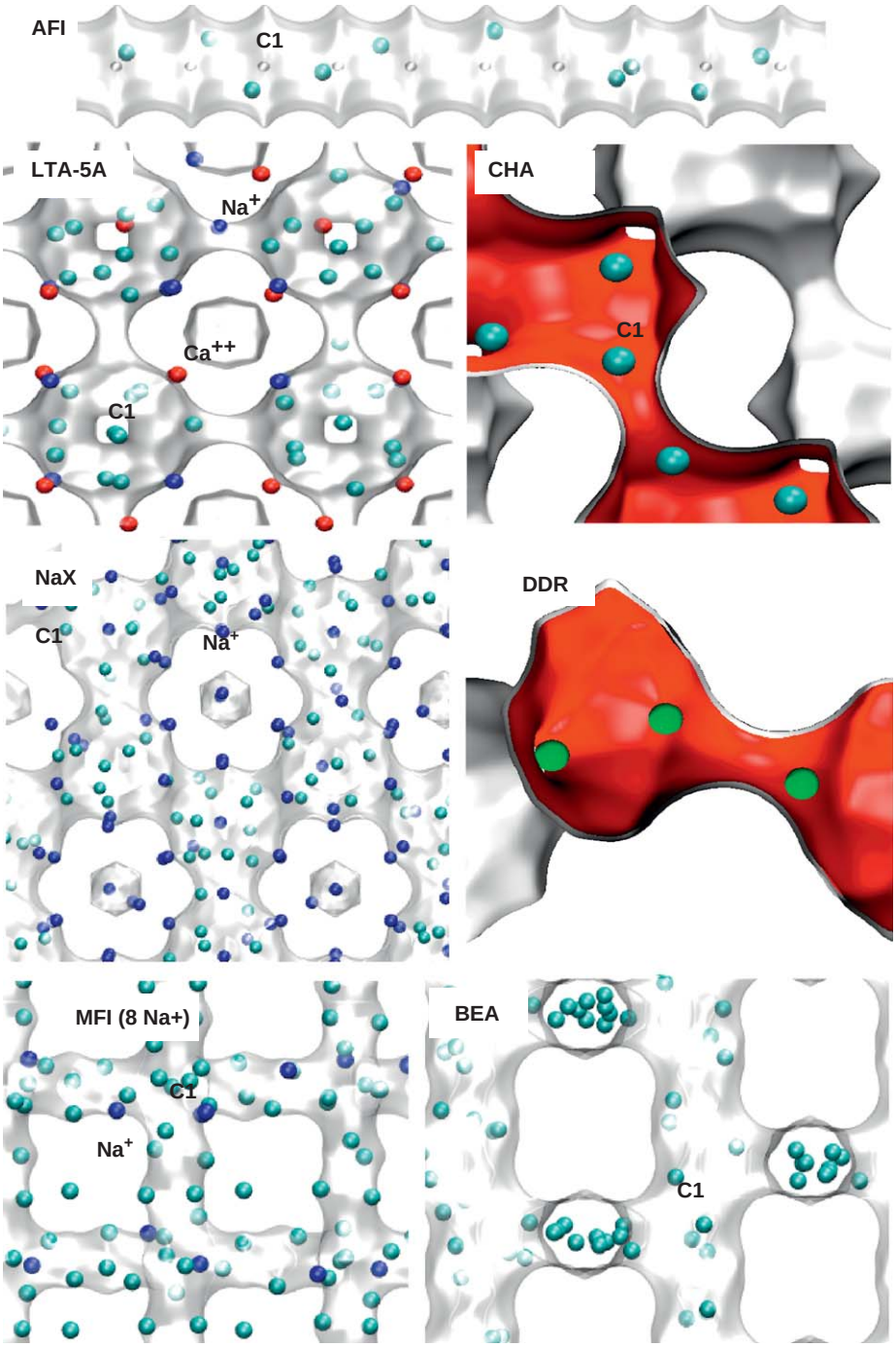

Fig. 2. Pore landscapes (iso-potential surfaces) of zeolites: AFI, LTA-5A, CHA, NaX, DDR, MFI (8 Na^+ per unit cell), and BEA.

on $Đ_i$ *and* self-diffusivities $D_{i,self}$ (Chempath et al., 2004; Krishna and van Baten, 2008a,b; Skoulidas et al., 2003). The prediction of the $Đ^*_{ij}$ demands a lot of input data, including the $c_{i,sat}$, that are accessible from molecular simulations, but not commonly from experiments.

The main objective of the present communication is to develop an alternate approach to modeling mixture diffusion in *micro*-pores using Eq. (1) with the c_i defined in terms of the accessible pore volumes inside the zeolites, MOFs, and COFs. By comparing (1) and (4) we find the inter-relation the two sets of exchange coefficients

$$c_{j,sat}Đ^*_{ij}/c_t = Đ_{ij} = Đ_{ji} = c_{i,sat}Đ^*_{ji}/c_t; \quad i,j = 1,2,\ldots,n \tag{8}$$

For micro-porous materials, the exchange coefficient $Đ_{ij}$ defined by Eq. (1) cannot be directly identified with the corresponding fluid phase diffusivity $Đ_{ij,fl}$ because the molecule–molecule interactions are also significantly influenced by molecule–wall interactions. However, we shall demonstrate that the characteristics of $Đ_{ij}$ are susceptible to a simpler physical interpretation than $Đ^*_{ij}$; this is the major rationale for the alternative, unified, treatment developed in this paper. We aim to show that the $Đ_{ij}$ for any guest–host structure combination is related to the fluid phase $Đ_{ij,fl}$ by a *constant* factor F defined as

$$F \equiv Đ_{ij}/Đ_{ij,fl} \tag{9}$$

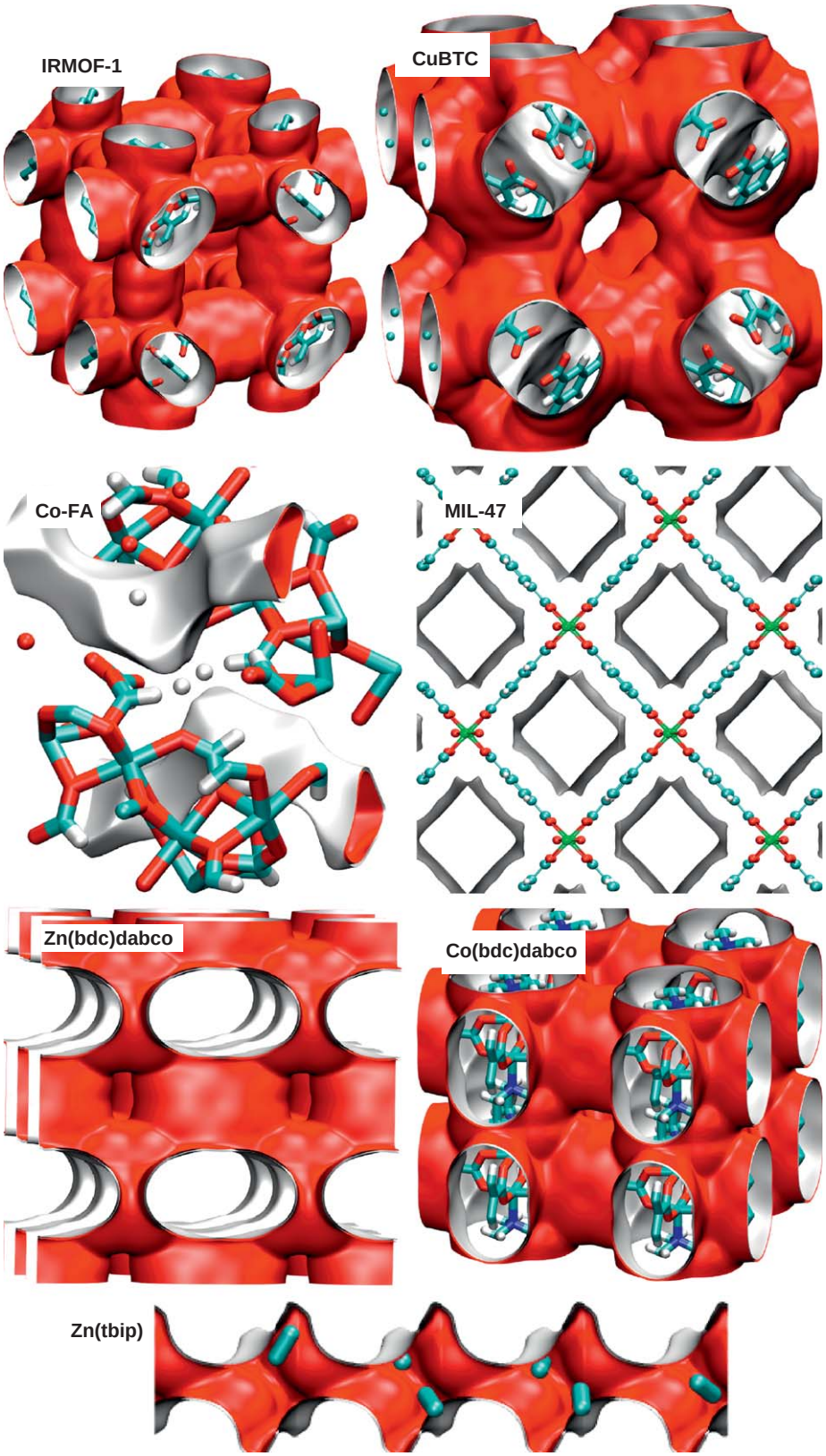

Fig. 3. Pore landscapes (iso-potential surfaces) of MOFs: IRMOF-1, CuBTC, Co-FA, MIL-47, Zn(bdc)dabco, Co(bdc)dabco, and Zn(tbip). The pore landscape of Mn-FA is similar to that of Co-FA. The structural information for the metal organic frameworks (MOFs) have been taken from various publications: Cobalt Formate (Co-FA) from Li et al.(2008); Manganese Formate (Mn-FA) from Dybtsev et al.(2004); Zn(bdc)dabco from Bárcia et al.(2008) and Lee et al. (2007); Co(bdc)dabco from Wang et al.(2008); MIL-47 from Alaerts et al. (2007), Finsy et al. (2008) and Barthelet et al.(2007); Zn(tbip) from Pan et al. (2006a,b); IRMOF-1 from Dubbeldam et al. (2007a,b); CuBTC from Chui et al. (1999) and Yang and Zhong (2006).

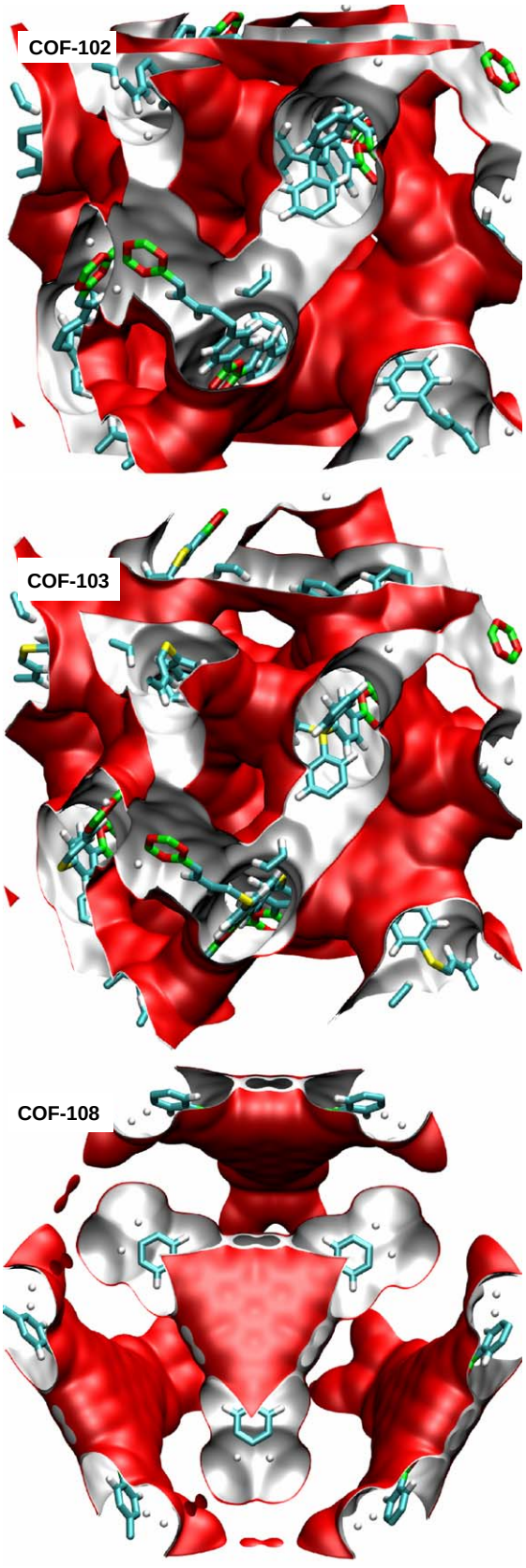

Fig. 4. Pore landscapes (iso-potential surfaces) of COFs: COF-102, COF-13, and COF-108. The structural information is from El-Kaderi et al. (2007)

that has a value smaller than unity. We also examine the variety of factors that influence the value of F, and suggest engineering estimation procedures for $Đ_{ij}$. We shall suggest interpolation procedures with a more transparent physical basis that aims to supplant the "empirical" Eq. (7).

To achieve our objectives we carried out MD simulations to determine the diffusivities $Đ_1$, $Đ_2$, and $Đ_{12}$ for the binary mixtures: neon (Ne)–argon (Ar), methane (C1)–Ar, C1–C2 (ethane), C1–C3 (propane), Ne–carbon dioxide (CO_2), Ar–CO_2, and C1–CO_2 in seven different zeolites (MFI, AFI, BEA, FAU, LTA, CHA, and DDR), eight different MOFs (IRMOF-1, CuBTC, Zn(bdc)dabco, Co(bdc)dabco, MIL-47, Co-FA, Mn-FA and Zn(tbip)), three different COFs (COF-102, COF-103, and COF-108), and cylindrical silica pores with diameters d_p ranging from 0.6 to 30 nm. Though the majority of simulations were with all-silica zeolites (Si/Al $= \infty$), a few simulations were carried out for unary diffusion in zeolites with finite Si/Al ratios to investigate the influence of the presence of cations: NaX (106 Si; 86 Al; 86 Na^{++}; Si/Al = 1.23), NaY (144 Si; 48 Al; 48 Na^{+}; Si/Al = 3), LTA-5A (96 Si; 96 Al; 32 Na^{+}; 32 Ca^{++}; Si/Al = 1), LTA-4A (96 Si; 96 Al; 96 Na^{+}; Si/Al = 1), and MFI (with 2Na^{+}, 4Na^{+}, 6Na^{+}, and 8Na^{+}).

Figs. 2–4 show the pore landscapes of the chosen zeolites, MOFs and COFs. The various structures are deliberately chosen to represent a wide variety of micro-pore topologies and connectivities: (a) one-dimensional channels (cylindrical silica pores, AFI, Zn(tbip), MIL-47, Co-FA, Mn-FA), (b) intersecting channels (MFI, BEA, Zn(bdc)dabco, Co(bdc)dabco), (c) cavities with large windows (FAU, NaX, NaY, IRMOF-1, CuBTC, COF-102, COF-103, and COF-108), and (d) cages separated by narrow windows (LTA, LTA-5A, LTA-4A, CHA, and DDR). The loadings within the pore space are varied to near saturation values. The accessible pore volumes of the various structures were determined using the helium probe insertion simulation technique described in the literature (Myers and Monson, 2002; Talu and Myers, 2001). The salient information, including the characteristic channel sizes, on the variety of structures investigated is listed in Table 1.

Additionally, we determined the fluid phase self-diffusivities $Đ_{ii,fl}$ of pure components along with the M–S diffusivity $Đ_{12,fl}$ for fluid mixtures. The entire data base of simulation results is available in the Supplementary material accompanying this publication; this material includes details of the MD simulation methodology, description of the force fields used, and simulation data. A selection of the simulation results is discussed below with the aim of drawing a variety of generic conclusions.

2. Exchange coefficient $Đ_{12}$ for binary mixture diffusion

We start by underlining the differences in mixture diffusion characteristics of micro- and meso-pores. For this purpose we consider the dependence of $Đ_{12}$ for an equimolar C1–Ar mixture on the total concentration c_t within cylindrical silica meso-pores of diameters $d_p = 2$, 3 and 4 nm; see Fig. 5a. The $Đ_{12,fl}$ for binary C1–Ar *fluid phase* mixture diffusion, obtained from independent MD simulations, is also presented in square symbols. At molar loadings $c_t < 4\,\text{kmol m}^{-3}$ the $Đ_{12,fl}$ decreases *linearly* with increasing c_t; this is the low-density gas limit. For $c_t > 8\,\text{kmol m}^{-3}$ we have high density fluid characteristics with a sharper decline in $Đ_{12,fl}$ with increasing c_t. We see that for meso-pore sizes of 2, 3, and 4 nm the $Đ_{12}$ can be identified with $Đ_{12,fl}$ over the entire loading range; this equality holds for all meso-pore sizes investigated, ranging to 30 nm. For $d_p = 0.6$, 0.75 and 1 nm, the $Đ_{12}$ are lower than the $Đ_{12,fl}$ values by a constant factor F; see Fig. 5b. The factor $F = 0.23$, 0.45, and 0.8 for $d_p = 0.6$, 0.75, and 1 nm, respectively, implying that the narrower the pore the larger is the departure from the fluid value $Đ_{12,fl}$. Put another way, the molecule–molecule interactions are influenced more significantly by the walls in narrower pores. Clearly the diffusion in

Table 1
Salient structural information on zeolites, MOFs and COFs.

Structure	Typical channel, cavity or window size	Pore volume fraction
MFI (all-silica)	Intersecting channels of 5.1–5.6 Å size	0.297
AFI	1D channels of 7.3 Å size	0.274
FAU (all-silica)	Cages separated by 7.4 Å size windows	0.44
NaY	Window size as for all-silica FAU	0.408
NaX	Window size as for all-silica FAU	0.4
CHA	Cages separated by 3.8 Å size windows	0.38
DDR	Cages separated by 3.6 Å×4.4 Å size windows	0.245
LTA (all-silica)	Cages separated by 4.1 Å size windows	0.4
LTA-5A	Window size lower than for all-silica LTA	0.38
BEA	Intersecting channels of two sizes: 7.1 and 5.6 Å	0.41
IRMOF-1	Two alternating, inter-connected, cavities of 10.9 and 14.3 Å with window size of 8 Å	0.81
CuBTC	Large cages are inter-connected by 9 Å windows of square cross-section. The large cages are also connected to tetrahedral-shaped pockets of ca. 6 Å size through triangular-shaped windows of ca. 4.6 Å size	0.75
MIL-47	One-dimensional channels of ca 8.5 Å diameter	0.61
Zn(bdc)dabco	Two types of channels: 7.5 Å×7.5 Å along the *a*-axis and channels of 3.8 Å×4.7 Å along *b*- and *c*-axis	0.66
Co(bdc)dabco	Channels similar to Zn(bdc)dabco	0.65
Co-FA	One dimensional zig-zag channels of 5.5 Å	0.25
Mn-FA	Adamantane-like cages of 5.5 Å diameter are connected to each other via a small window of approximately 4.5 Å to form a 1D zig-zag channels	0.3
Zn(tbip)	One dimensional channels of 4.5 Å size	0.175
COF-102	Cavity of size 8.9 Å	0.8
COF-103	Cavity of size 9.6 Å	0.82
COF-108	Two cavities, of sizes 15.2 and 29.6 Å	0.93

The data on pore volume fraction is obtained using the helium probe insertion simulation technique (Myers and Monson, 2002; Talu and Myers, 2001).

pores with $d_p < 2$ nm, needs to be approached in a manner different to that for $d_p > 2$ nm in size. The important message to emerge from the silica pore simulation results in Fig. 5 is that if the factor F can be estimated, then this paves the way to estimating the $Đ_{12}$ in micro-pores.

A representative selection of the MD simulation results obtained for the $Đ_{12}$ for diffusion of equimolar Ne–Ar, C1–Ar, C1–C2, and Ne–CO_2 mixtures in zeolites, MOFs, and COFs are summarized in Fig. 6. It is remarkable to note the parallelism in the loading dependence of $Đ_{12}$ for structures of such diverse topologies; in all cases the $Đ_{12}$ is related to the corresponding fluid $Đ_{12,fl}$ by a *constant* factor F, which depends on the particular guest–host combination. This is already a useful result because the loading dependence of $Đ_{12}$ is the same as that for the fluid phase $Đ_{12,fl}$ and therefore this can be estimated in an independent manner. Let us examine whether the trend in the factor F can be understood and rationalized.

Open structures such as COFs, IRMOF-1, and CuBTC with high fractional pore volume, ϕ, in the range 0.7–0.93 and cavity sizes larger than about 0.8 nm, have $F > 0.55$. Generally speaking, for such open structures with wide windows separating cavities, $Đ_{12}$ is easy to estimate but such materials are mainly destined for storage applications (Czaja et al., 2009; El-Kaderi et al., 2007; Férey, 2008; Yaghi, 2007), where diffusion issues are not entirely relevant.

Zn(bdc)dabco and Co(bdc)dabco are iso-structural and consist of a set of intersecting channels with two different channel sizes, large channels of 0.75×0.75 nm, and small channels of 0.38 nm×0.47 nm (Bárcia et al., 2008; Dubbeldam et al., 2008; Wang et al., 2008) (cf. Fig. 3). The stronger confinement in the smaller channels leads to a low value of $F < 0.3$. Cobalt formate (Co-FA), that consists of one-dimensional zig-zag channels of 0.5–0.6 nm size, has extremely low value of $F = 0.04$. Correlations in molecular jumps are particularly strong due to both strong confinement of guest molecules, and the poor connectivity of 1D channels of Co–FA; these two factor combine to yield low $Đ_{12}$ and F values.

For zeolites, the general trend is that F is higher for large-pore FAU and AFI, than for medium pore MFI. BEA, that consists of intersecting channels of two different sizes, large pore and medium pore, has F values higher than for MFI but lower than that of FAU.

Drawing clues from the results in Fig. 5 for cylindrical silica pores, we anticipate the factor F to correlate with characteristic size of the channels or windows in the micro-porous structures. We also expect the characteristic size of the guest molecules to be influential; for this purpose we take the Lennard-Jones size parameter σ to be characteristic of the size of the guest species. For C1, Ar, and Ne the values of σ are 0.37, 0.34, and 0.28 nm, respectively; see force field details in the Supplementary material. For the equimolar Ne–Ar and C1–Ar mixtures we take the arithmetic average of the constituent species σ's as the characteristic measure of guest size. Using the characteristic channel dimensions listed in Table 1 we constructed the plot in Fig. 7a, wherein F is plotted against the degree of confinement, defined as the ratio of the average σ to that of the channel dimension. Generally speaking, F is seen to decrease with the degree of confinement This is a rational result because it is to be expected that in more confined spaces, the molecules will "interact" more strongly with one another, leading to stronger correlations in molecular jumps, and consequently a lower exchange diffusivity $Đ_{12}$. The exception to the general trend in Fig. 7a is the "rogue" behavior for diffusion in LTA, CHA and DDR (the data points are encircled). These three zeolites have cages separated by narrow 0.36–0.44 nm sized windows that allow only one molecule at a time to hop from one cage to another. The inter-cage hopping is therefore poorly correlated (Krishna and van Baten, 2008a,b), resulting in a much higher $Đ_{12}$, and therefore F, than anticipated for the narrow window size. As pointed out in earlier publications, for all such zeolite structures correlations are weak, though not of negligible importance for modeling experimental mixture permeation across zeolite membranes (Krishna et al., 2008; Li et al., 2007b). We dwell further on correlation effects in more detail later in this paper.

3. M–S diffusivity $Đ_i$

Though Eq. (1) are applied in the current paper to describe diffusion in both meso- and micro-pores, there are a number of important differences in the underlying physics that determine the $Đ_i$, representing molecule–wall interactions. We now compare and contrast the characteristics of this parameter in micro- and meso-pores.

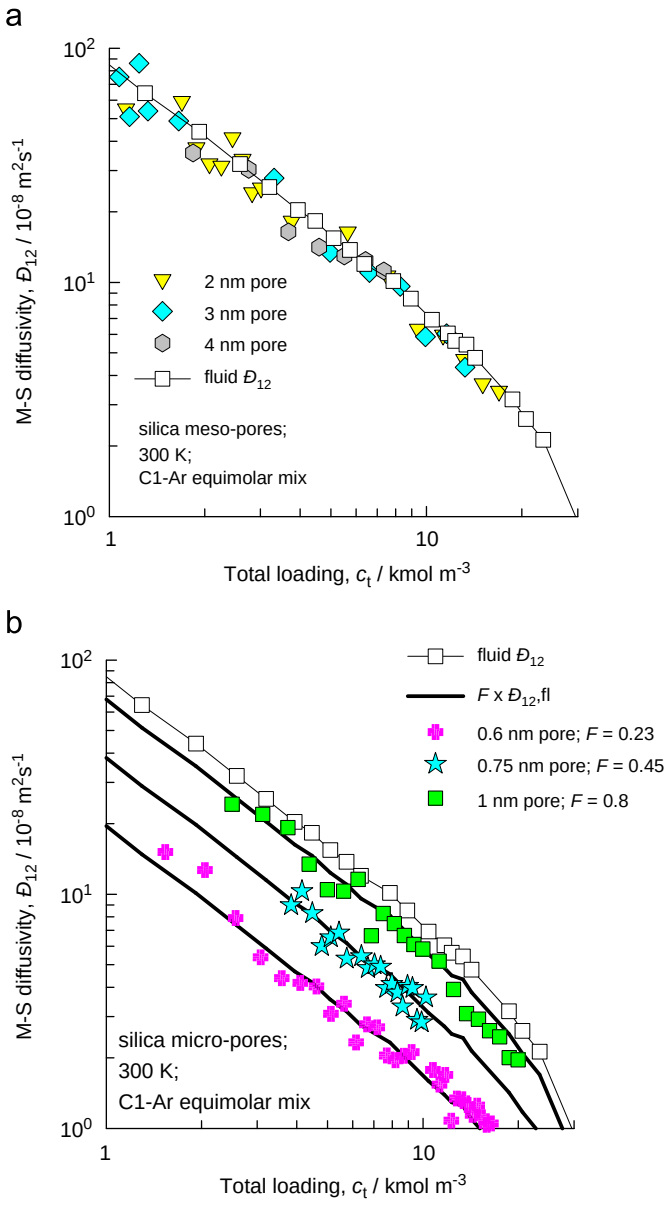

Fig. 5. The M–S binary exchange coefficients $Đ_{12}$, for diffusion of equimolar ($c_1 = c_2$) binary mixture of C1 (1) and Ar (2) in cylindrical silica pores with (a) $d_p = 2$, 3 and 4 nm, and (b) $d_p = 0.6$, 0.75, and 1 nm at 300 K as a function of the total fluids concentration, c_t. The $Đ_{12,fl}$ for binary C1-Ar *fluid phase* mixture diffusion, obtained from independent MD simulations, is also presented in square symbols, along with lines that are a fraction F times $Đ_{12,fl}$. The data for 1–4 nm are from Krishna and van Baten (2009a); simulations for the 0.6, and 0.75 nm pore were carried out using the same strategy, details are available in the Supplementary material.

For micro-pore diffusion, previous work (Chempath et al., 2004; Krishna and van Baten, 2005b, 2008a,b; Skoulidas et al., 2003) has shown that the $Đ_i$ in Eq. (1) for *mixture* diffusion can be identified with the corresponding value for *unary* diffusion provided the latter is evaluated at the total mixture occupancy

$$\theta = \theta_1 + \theta_2 = \frac{c_1}{c_{1,sat}} + \frac{c_2}{c_{2,sat}} \tag{10}$$

For meso-pores, the $Đ_i$ in the mixture can be identified with the unary $Đ_i$ evaluated at the total mixture loading c_t (Krishna and van Baten, 2009a).

Fig. 8a and b shows the M–S diffusivities $Đ_i$, for methane in (a) zeolites, (b) MOFs, and COFs as a function of the concentration, c_i. The zero-loading value $Đ_i(0)$ decreases strongly, by a few orders of magnitude, with increasing the degree of confinement. The wide variety in $Đ_i - c_i$ dependencies in the various structures is worthy of note. Generally speaking, $Đ_i$ decreases with increase in the loading c_i; this is due to the reduction in the number of vacant sites that molecules can hop to. As the saturation loading $c_{i,sat}$ is approached, the $Đ_i$ tends to decrease sharply. A similar sharp decline is also observed for the self-diffusivities of pure fluids, $Đ_{ii,fl}$. This implies that the self-diffusivity of densely packed fluid phase is the lower limiting value for $Đ_i$ as $c_{i,sat}$ is approached. Indeed, Barrer and Sutherland (1956) and, subsequently, Golden and Sircar (1994) have used the molar density of the liquid phase as an estimate of $c_{i,sat}$ for a variety of guest species in zeolites. This procedure is particularly useful, and necessary, for the estimation of $c_{i,sat}$ for light gases that have poor adsorption strength; in such cases it is difficult, if not impossible, to attain saturation conditions in adsorption isotherm measurements even when operating at high pressures (Li et al., 2007a,b).

For methane the saturation capacity in different micro-porous structures $c_{i,sat} \approx 31\,\text{kmol m}^{-3}$, with about a 15% variation; this is evidenced by comparing the isotherms for C1 for a wide variety of structures; see Fig. 9. Expressed in terms of mol per kg of framework, the saturation capacities of C1 in various zeolites show a significantly wider variation, ranging from 4 for MFI to 11.5 for FAU (Krishna and van Baten, 2008a). Adopting Eq. (1) with c_i in terms of accessible pore volumes is advantageous from the point of view of estimating the $c_{i,sat}$, required in the use of the Reed and Ehrlich model for modeling the $Đ_i - c_i$ dependence (Krishna and van Baten, 2008b; Reed and Ehrlich, 1981); this model has also been used to describe the surface transport resistance of MOF crystals (Heinke et al., 2009; Tzoulaki et al., 2009).

In some cases the isotherm shows inflection behavior. For Co–FA and Mn–FA, inflection occurs at a loading corresponding to one molecule of methane per channel segment of the one-dimensional zig-zag channels of these structures (Krishna and van Baten, 2009c); see Fig. 9d. To attain higher loadings two methane molecules need to occupy one channel segment; this requires an extra "push" and results in inflection. The consequence of creating additional adsorption sites is an *increase* in the $Đ_i$ at loadings > 1 molecule per channel segment, which corresponds with $c_i \approx 12$ and $16\,\text{kmol m}^{-3}$ for Mn–FA and Co–FA, respectively; see Fig. 8b.

There is experimental evidence of the strong influence of isotherm inflection on $Đ_i - c_i$ dependence in MFI and CuBTC (Chmelik et al., 2008, 2009; Jobic et al., 2006). For MOFs and COFs, framework flexibility could be of special importance and MD simulations have shown a significant influence on both the magnitude and the loading dependence of the diffusivities (Amirjalayer et al., 2007; Greathouse and Allendorf, 2008; Seehamart et al., 2009). Generally speaking, framework flexibility issues are of lesser importance in zeolites (Zimmermann et al., 2007).

For diffusion in LTA, CHA, and DDR that consist of cages separated by narrow windows, $Đ_i$ increases with c_i because of the reduction in the free-energy barrier for inter-cage hopping (Beerdsen et al., 2005, 2006). Experiments for permeation across DDR and CHA membranes can be properly interpreted only if the increase in the $Đ_i$ is properly accounted for (Krishna and van Baten, 2008c; Krishna et al., 2007; Li et al., 2007b; van den Bergh et al., 2008, 2007).

The presence of cations such as Na^+ and Ca^{++} in LTA leads to a significant reduction in diffusivity; this is illustrated in Fig. 8c that compares the diffusivities of LTA (all-silica), with LTA-5A (96 Si, 96 Al, 32 Na^+, 32 Ca^{++}) at three different temperatures for a range of c_i values. Generally speaking, cations occupy sites that partially block the 8-membered ring window (Fritzsche et al., 1995; Hedin et al., 2008, 2007). The activation energy for C1 diffusion in LTA-5A is also significantly higher than for LTA (all silica); see Fig. 8d. The reason for this is the significantly higher adsorption strength in LTA-5A due to the presence of cations.

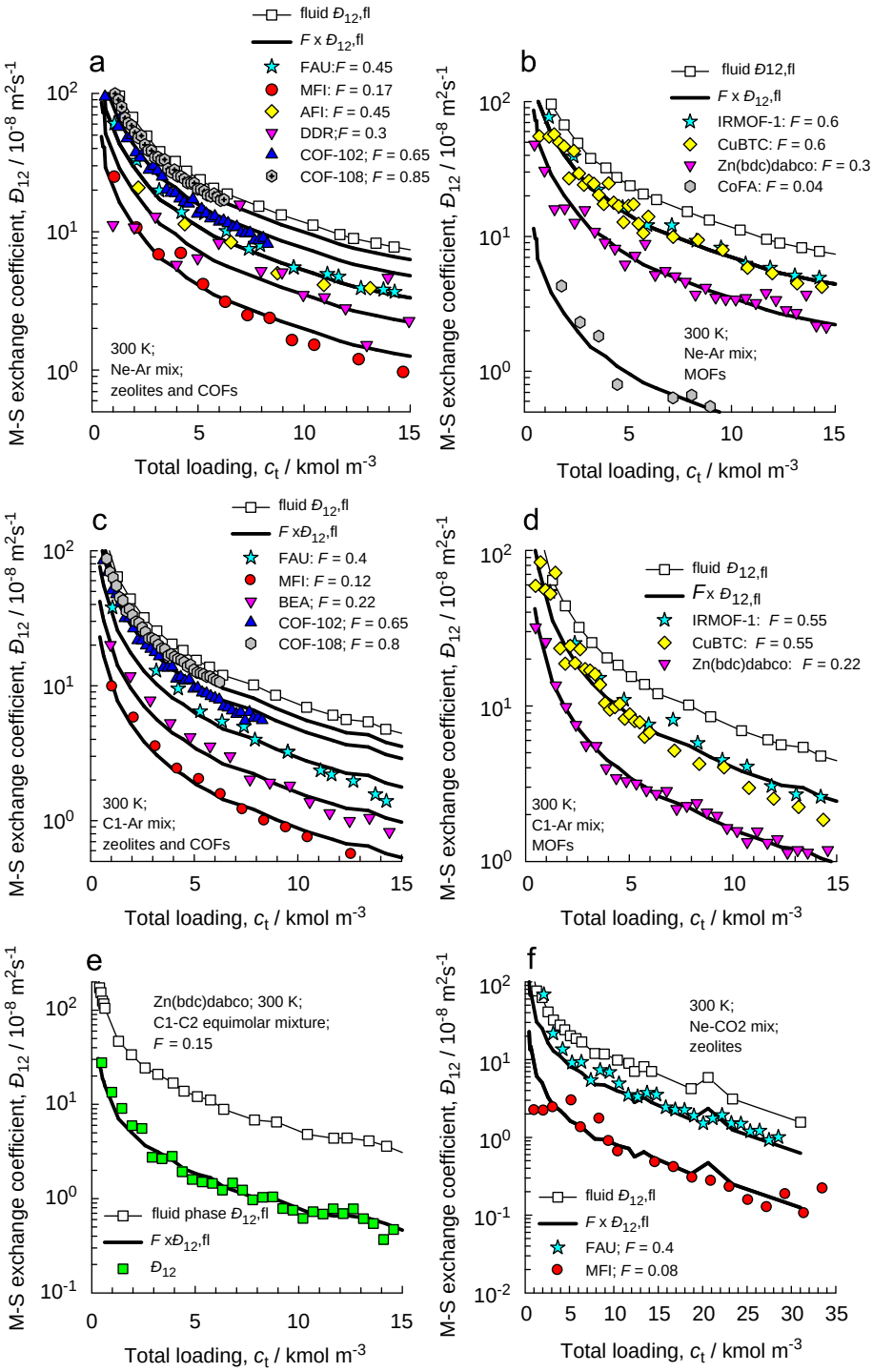

Fig. 6. The M–S binary exchange coefficients $Đ_{12}$, for diffusion of equimolar ($c_1 = c_2$) binary mixtures (a,b) Ne–Ar, (c,d) C1–Ar, (e) C1–C2, and (f) Ne–CO_2 mixtures in zeolites, MOFs, and COFs at 300 K as a function of the total concentration, c_t. The $Đ_{12,fl}$ for binary *fluid phase* mixture diffusion, obtained from independent MD simulations, are also presented in square symbols, along with continuous solid lines that represent the fraction F times $Đ_{12,fl}$. Note that only a selection of the simulation results are presented here; the complete set of results are available in the supplementary material.

The presence of cations also causes a significant reduction of $Đ_i$ in MFI because the channels become more constricted. On the other hand, for diffusion in more open structures such as FAU there is a relatively small influence due to the influence of cations. More detailed data and information on the influence of cations is available in the Supplementary material.

Since the $Đ_i$ for micro-pore diffusion reflects an *activated* surface diffusion process, the zero-loading diffusivities $Đ_i(0)$ follow an Arrhenius temperature dependence (Kärger and Ruthven, 1992; Krishna and van Baten, 2009b). The activation energy is, in general, dependent on the loading (Krishna and van Baten, 2009b).

The $Đ_i - c_i$ dependence for meso-pores is fundamentally different from that for micro-pores. This is underlined in the MD simulations results for diffusion of methane in cylindrical silica pores of diameters $d_p = 0.6$, 2, 3, 4 and 5.8 nm as a function of the fluids concentration, c_i; see Fig. 10a. For the 0.6 nm micro-pore $Đ_i$ declines linearly

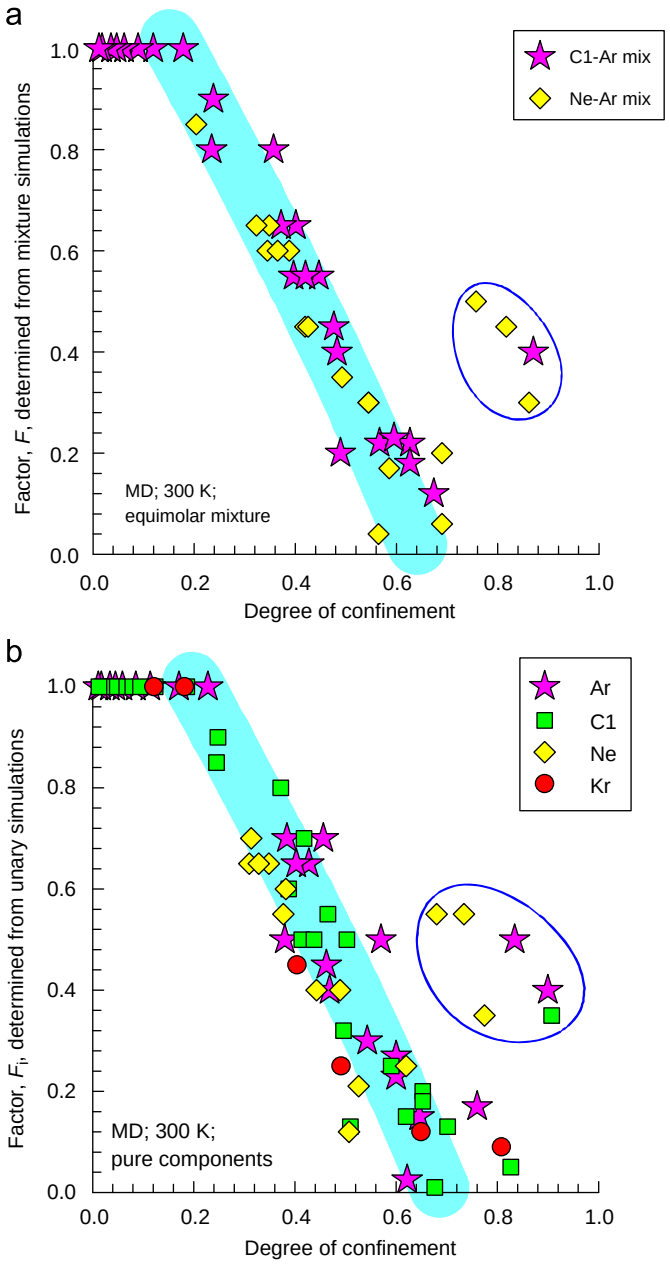

Fig. 7. (a) Factor F determined from mixture simulations, and (b) factor F_i determined from unary simulations, both expressed as a function of the degree of confinement of guest molecules within the channels. The characteristic sizes are indicated in Table 1. For MFI, BEA, Zn(bdc)dabco, and Co(bdc)dabco the average channel dimensions of 0.53, 0.63, 0.57, and 0.57 nm were used. For FAU LTA, CHA, DDR, CuBTC, IRMOF-1 the window sizes were used. For COF-108 the smaller cavity size of 1.52 nm was used. The data presented includes those for cylindrical silica pores. The data for CHA, DDR, and LTA are encircled

with c_i due to a reduction the number of vacant adsorption sites; this is a characteristic feature of surface diffusion, which is an activated process. For the meso-pores $Đ_i$ increases with c_i due to the additional contribution of viscous flow: $d_p^2 c_i RT/32\eta_i$, which contribution increases with the square of the pore diameter.

Consider the cylindrical 3 nm silica pore; from Fig. 10a we note that $Đ_i(0) = 16\times10^{-8}$ m^2 s^{-1}, which value is significantly lower than the Knudsen diffusivity $D_{i,Kn} = 32\times10^{-8}$ m^2 s^{-1}; the lowering is due to significant adsorption of methane. In order to underline the strong influence of adsorption we carried out MD simulations for methane diffusion in the 3 nm pore in which the Lennard-Jones parameter for energy of interaction between C1 and the O atoms of the silica pore are varied from the base case value of 115 K in five steps: $\varepsilon/k_B = 64.6$, 91.4, 115 (base case), 129, and 158 K; see Fig. 10b (in these sensitivity studies, the Lennard-Jones size parameter σ was held constant). With increased ε/k_B the adsorption strength increases, and consequently the contribution of surface diffusion increases at the expense of the Knudsen contribution; this leads to a strong *decrease* in the $Đ_i$. For the lowest value $\varepsilon/k_B = 64.6$ K, signifying negligible adsorption, we note that $Đ_i(0) \approx D_{i,Kn} = 32\times10^{-8}$ m^2 s^{-1}. Engineering design calculations assuming predominantly Knudsen transport become progressively worse as the strength of adsorption increases.

Increasing temperature reduces the adsorption strength, and therefore a reduction in ε/k_BT results in a closer match of $Đ_i(0)$ with $D_{i,Kn}$; this is confirmed by the data for C1 and Ar in 2 and 3 nm pores; see Fig. 10c. It is interesting to note the overlap in the data for C1 and Ar, suggesting that the graph has a generic character. In Fig. 10d we plot $Đ_i(0)$ vs. $D_{i,Kn}$ for C1 and Ar in 2 and 3 nm pores at various T; we note that for high T, the two sets coincide with the parity line, and that the deviations are higher at lower T. We also note that the data do not run parallel to the parity line, suggesting that for meso-pore diffusion, the $Đ_i(0) - T$ dependence is complex. For non-adsorbing molecules we have a $\sqrt{T}$ dependence as a consequence of Knudsen behavior, but for cases with significant adsorption the T-dependence has an Arrhenius character (Bhatia and Nicholson, 2003; Krishna and van Baten, 2009a).

Within regular micro-porous structures there is a possibility of a non-monotonous dependence of the diffusivity with molecular chain length of n-alkanes due to incommensurate–commensurate adsorption effects; this has been demonstrated both in MD simulations (Dubbeldam et al., 2003; Dubbeldam and Smit, 2003; Krishna and van Baten, 2009c) and experiment (Jobic et al., 2004). Corresponding incommensurate adsorption effects have not been reported in meso-porous materials; these are also not expected to occur.

In meso-porous materials the phenomenon of capillary condensation, and adsorption hysteresis are commonly observed; these have an impact on the diffusion process (Naumov et al., 2007; Valiullin et al., 2006). For diffusion of n-alkanes in CuBTC crystals, there is some experimental evidence of diffusion being influenced by phase transition phenomena (Chmelik et al., 2009).

4. Self-exchange coefficient $Đ_{ii}$

Let us apply Eq. (1) to equimolar diffusion ($N_1+N_2=0$) in a system consisting of two species, tagged and un-tagged, that are identical with respect to diffusional properties:

$$-\frac{c_1}{RT}\nabla\mu_1 = \frac{(x_1+x_2)N_1}{Đ_{11}} + \frac{N_1}{Đ_1} = \left(\frac{1}{Đ_{11}} + \frac{1}{Đ_1}\right)N_1 \tag{11}$$

Eq. (11) defines the self-diffusivity $D_{i,self}$ within a pore

$$-\frac{c_i}{RT}\nabla\mu_i = \frac{N_i}{D_{i,self}} \tag{12}$$

and so we derive the expression

$$\frac{1}{D_{i,self}} = \frac{1}{Đ_i} + \frac{1}{Đ_{ii}}; \quad i = 1,2 \tag{13}$$

The $Đ_{ii}$ in Eq. (13) is the self-exchange coefficient within the pore and can be evaluated from MD simulations of both $Đ_i$, and $D_{i,self}$. The $Đ_{ii}$ is related to $Đ^*_{ii}$, defined in the earlier published M–S formulations in terms of the vacancy θ_i (Krishna and van Baten, 2005b)

$$Đ^*_{ii}/\theta_i = Đ_{ii} \tag{14}$$

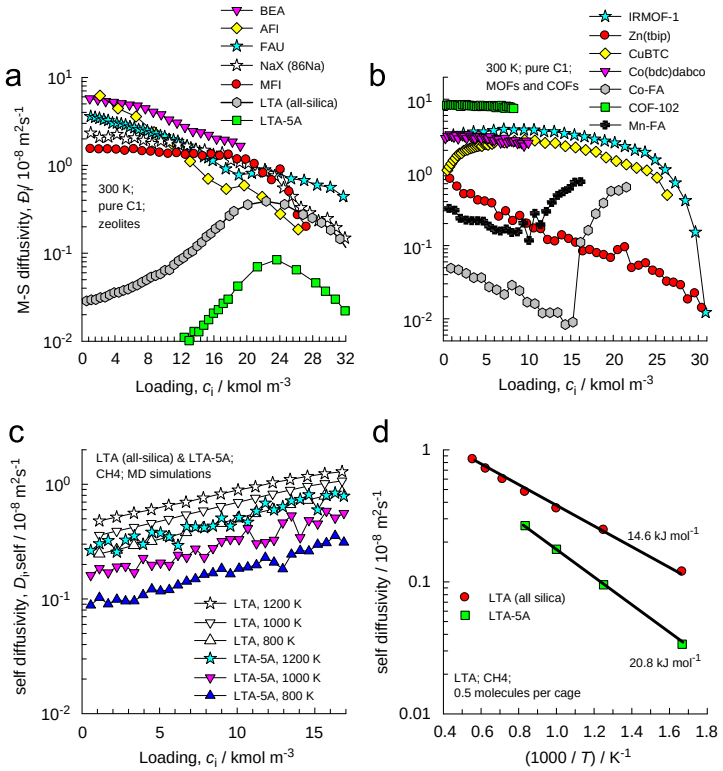

Fig. 8. The M–S diffusivities $Đ_i$, for pure methane in (a) zeolites, (b) MOFs, and COFs at 300 K as a function of the concentration, c_i. (c) Influence of cations on the diffusivity of C1 in LTA (all-silica), and LTA-5A (96 Si, 96 Al, 32 Na^+, 32 Ca^{++}) for a range of loadings at 800 K, 1000 K, and 1200 K. (d) Comparison of activation energies for diffusion of C1 in LTA (all-silica), and LTA-5A.

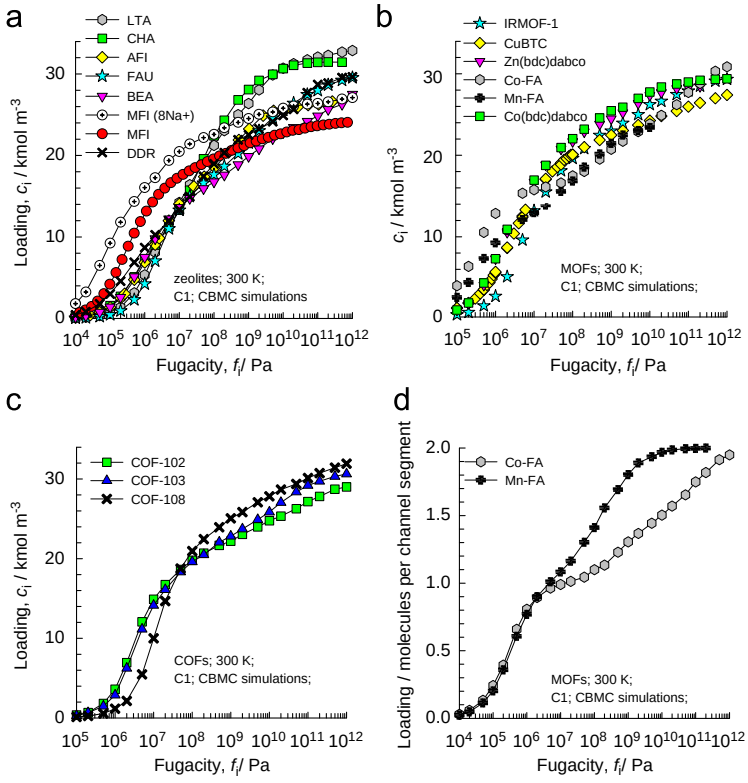

Fig. 9. CBMC simulations of adsorption isotherms for pure methane in (a) zeolites, (b) MOFs, and (c) COFs at 300 K as a function of the fluid phase fugacity, f_1. (d) Isotherms for Co-FA, and Mn-FA with loadings expressed in terms of molecules per segment of the zig-zag channels.

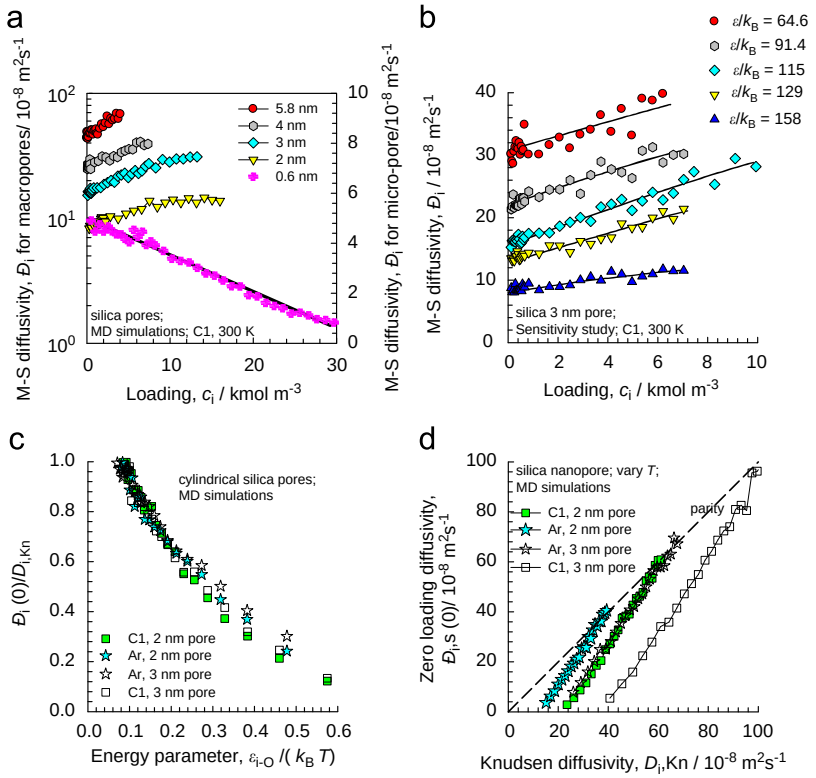

Fig. 10. (a) M–S diffusivity $Đ_i$, for diffusion of pure methane in cylindrical silica pores with $d_p = 0.6$, 2, 3, 4 and 5.8 nm at 300 K as a function of the fluids concentration, c_i. The data for $d_p = 2$, 3, 4, and 5.8 nm are from Krishna and van Baten (2009a); simulations for the $d_p = 0.6$ nm pore are from this work. Note that the 0.6 nm pore results are plotted with the right y-axis on a linear scale. (b) Sensitivity study of the M–S diffusivity $Đ_i$, for diffusion of pure methane in cylindrical silica pore of 3 nm at 300 K as a function of the fluids concentration, c_i. The Lennard-Jones parameter for energy of interaction between C1 and the O atoms of the silica pore are varied from the base case value of 115 K: $\varepsilon/k_B = 64.6$ K, 91.4 K, 115 K (base case), 129 K, and 158 K. (c) MD data for $Đ(0)/D_{i,Kn}$ as a function of the energy parameter ε/k_BT for diffusion of C1, and Ar at various temperatures in 2 nm, and 3 nm cylindrical silica pores. (d) MD data on $Đ(0)$ for C1 and Ar in 2 nm, and 3 nm silica pores at a variety of temperatures plotted against the Knudsen diffusivity $D_{i,Kn}$.

Fig. 11a shows the self exchange coefficients $Đ_{ii}$, for diffusion of methane in cylindrical silica meso-pores with $d_p = 2$, 3 and 4 nm as a function of the fluids concentration, c_i. The $Đ_{ii,fl}$ for *fluid phase* self diffusion, obtained from independent MD simulations, is also presented in square symbols. We note the good agreement of $Đ_{ii}$ with $Đ_{ii,fl}$ for the entire range of c_i; similar agreement holds for larger meso-pore sizes ranging to 30 nm. For the 0.6, 0.75 and 1 nm pore sizes, the $Đ_{ii}$ are lower than the $Đ_{ii,fl}$ values by a constant factor F_i defined by

$$F_i \equiv Đ_{ii}/Đ_{ii,fl} \tag{15}$$

as shown in Fig. 11b. The factor $F_i = 0.15$, 0.32, and 0.8 for $d_p = 0.6$, 0.75, and 1 nm pores, respectively, implying that the narrower the pore the larger is the departure from the fluid value $Đ_{ii,fl}$; this parallels the results for mixture diffusion presented in Fig. 5b. An analogous picture holds for Ar; see Fig. 11c and d. The F_i values for $d_p = 0.6$, and 0.75 nm pores are higher than for C1 because of the smaller degree of confinement within the silica pores.

The convenient relation $Đ_{ii} = F_i \times Đ_{ii,fl}$ is found to hold for all guest–host combinations investigated, and is illustrated by a selection of $Đ_{ii}$ data for pure Ne, C1 and Ar in zeolites, MOFs, and COFs; see Fig. 12. It is remarkable to note the parallelism of the $Đ_{ii} - c_i$ dependencies in various structures despite the strong differences in the corresponding $Đ_i - c_i$ relations. In open structures such as FAU, the presence of cations has no significant influence on the $Đ_{ii}$, whereas there is a significant reduction in $Đ_{ii}$ in MFI due to the higher degree of confinement caused by the presence of cations. For diffusion of C1 in LTA-5A, the differences between the self- and M–S-diffusivities were indistinguishable and therefore the $Đ_{ii}$ are indeterminate. More information on the influence of cations on $Đ_{ii}$ is available in the Supplementary material.

The factor F_i determined from unary simulations are collated and plotted against the degree of confinement in Fig. 7b. The trend is similar to those obtained from binary mixture simulations (cf. Fig. 7a), as is to be expected. The results for LTA, CHA and DDR (encircled symbols) exhibit rogue behavior, the reasons for which have already been discussed earlier.

Diffusion in carbon nanotubes (CNTs) is a special case; the walls of CNTs are smooth and $Đ_i \gg D_{i,self}$ yielding $D_{i,self} \approx Đ_{ii,fl} \approx Đ_{ii,fl}$ for CNT(20,0) that has a diameter of 1.56 nm (Krishna and van Baten, 2006).

5. Degree of correlations $Đ_i/Đ_{ii}$

The $Đ_{ii}$ encapsulate the influence of correlation effects in unary diffusion. The larger the value of the M–S diffusivity $Đ_i$ with respect to self-exchange $Đ_{ii}$ the stronger are the consequences of correlation effects, and we may consider the ratio $Đ_i/Đ_{ii}$ as a measure of the degree of correlations.

For meso-pores, i.e. $d_p > 2$ nm, the factor $F_i = 1$, and consequently the ratio $Đ_i/Đ_{ii}$ progressively increases with increasing pore diameter; see Fig. 13a. This implies that correlation effects are stronger in larger diameter meso-pores. In separation applications, correlation effects have the effect of slowing down the more mobile species and

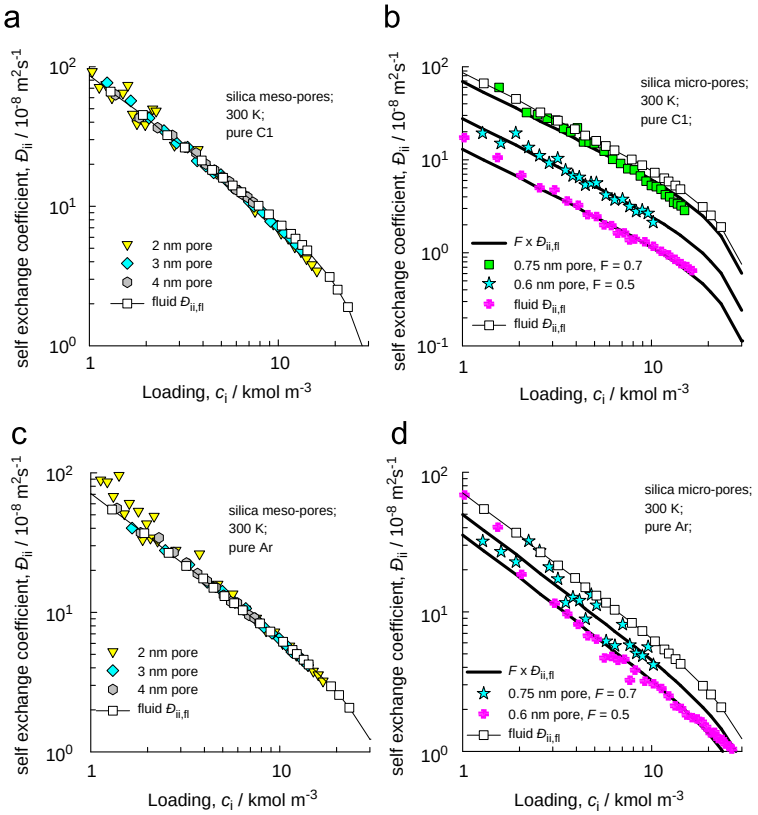

Fig. 11. Self exchange coefficients $Đ_{ii}$, for diffusion of (a,b) pure methane, and (c,d) pure Ar in cylindrical silica pores with (a,c) $d_p = 2$, 3 and 4 nm, and (b,d) $d_p = 0.6$, 0.75, and 1 nm at 300 K as a function of the fluids concentration, c_i. The $Đ_{ii,fl}$ for *fluid phase* self diffusion, obtained from independent MD simulations, is also presented in square symbols, along with lines that are a fraction F_i times $Đ_{ii,fl}$. The data for 1–4 nm are from Krishna and van Baten (2009a); simulations for the 0.6, and 0.75 nm pore were carried out using the same strategy, details are available in the supplementary material.

speeding-up the tardy ones; consequently the separation selectivity is reduced. Broadly speaking, therefore, smaller pore diameters are to be preferred in separation applications. The corresponding data for $Đ_i/Đ_{ii}$ for a small selection of micro-pore structures BEA, MFI, FAU, NaX, NaY, LTA, MIL-47, CuBTC, Zn(bdc)dabco and IRMOF-1 are shown in Fig. 13b and c. Correlation effects are stronger in 1D, and intersecting channel structures such as MIL-47, BEA, MFI, and Zn(bdc)dabco than in "open" structures such as FAU, NaX, NaY, CuBTC, and IRMOF-1. Correlation effects are particularly severe in 1D structures in which single file diffusion of the guest species occurs (Kärger and Ruthven, 1992); generally speaking 1D structures are not viable candidates for separation applications. It is interesting to note that $Đ_i/Đ_{ii}$ is practically identical for FAU, NaX, and NaY; the cations do not influence the degree of correlations for methane diffusion in such open structures. An analogous result is also obtained for ethane and propane. For LTA, $Đ_i/Đ_{ii} \approx 0$ for loadings below about 10 kmol m^{-3}, suggesting that correlations are of negligible importance. For LTA-5A, $Đ_i/Đ_{ii} \approx 0$ holds for the entire range of loadings.

With increasing degree of correlations, the first member on the right side of Eq. (1) becomes of increasing importance. Conversely, in cage structures such as LTA and CHA, the inter-cage hopping of molecules across the narrow windows are practically uncorrelated; for such structures the use of *uncoupled* flux relations, ignoring the first right member of Eq. (1), is a reasonable approximation for engineering design. The uncoupled flux relations were first suggested by Habgood (1958) to model uptake experiments in LTA-4A. Lack of coupling is attractive in separation applications, because there is negligible slowing-down of the faster species (Krishna et al., 2008; Li et al., 2007b).

Comparing the data in Fig. 13a–c we conclude that micro-porous materials are superior in separation applications due to weaker correlation effects than in meso-pores.

6. Estimation of $Đ_{12}$ for micro-porous structures

There are two ways to estimate the $Đ_{12}$ for micro-porous structures. In the first approach we proceed via the fluid phase $Đ_{ij,fl}$. The $Đ_{ij,fl}$ for fluid mixtures can be estimated from unary *self*-diffusivities $Đ_{ii,fl}$ using the Darken (1948) relations (Krishna and van Baten, 2005a):

$$Đ_{12,fl} = x_1 Đ_{11,fl} + x_2 Đ_{22,fl} \tag{16}$$

We also note, in passing, that the formula (16) has been misprinted in Krishna and van Baten (2009a). The $Đ_{ii,fl}$ are more accessible, both experimentally (Bidlack and Anderson, 1964; Helbaek et al., 1996; Shieh and Lyons, 1969) and from MD simulations (Dysthe et al., 1999; Fernández et al., 2004; Frenkel and Smit, 2002; Goo et al., 2002; Merzliak and Pfennig, 2004; Wheeler and Newman, 2004; Zabala et al., 2008) than the $Đ_{ij}$. Procedures for estimation of the $Đ_{ii,fl}$ are available in Poling et al. (2001) and Yu and Gao (2000). To illustrate the accuracy of Eq. (16), Fig. 14 shows MD simulations of self diffusivities $Đ_{ii,fl}$ of pure components, along with the $Đ_{12}$ for a variety of equimolar binary fluid mixtures as a function of the total fluids concentration, c_t. The calculations of $Đ_{12,fl}$ according to Eq. (16), shown by the continuous solid line, are in good agreement with the MD simulated values of $Đ_{12,fl}$ over the entire range of concentrations.

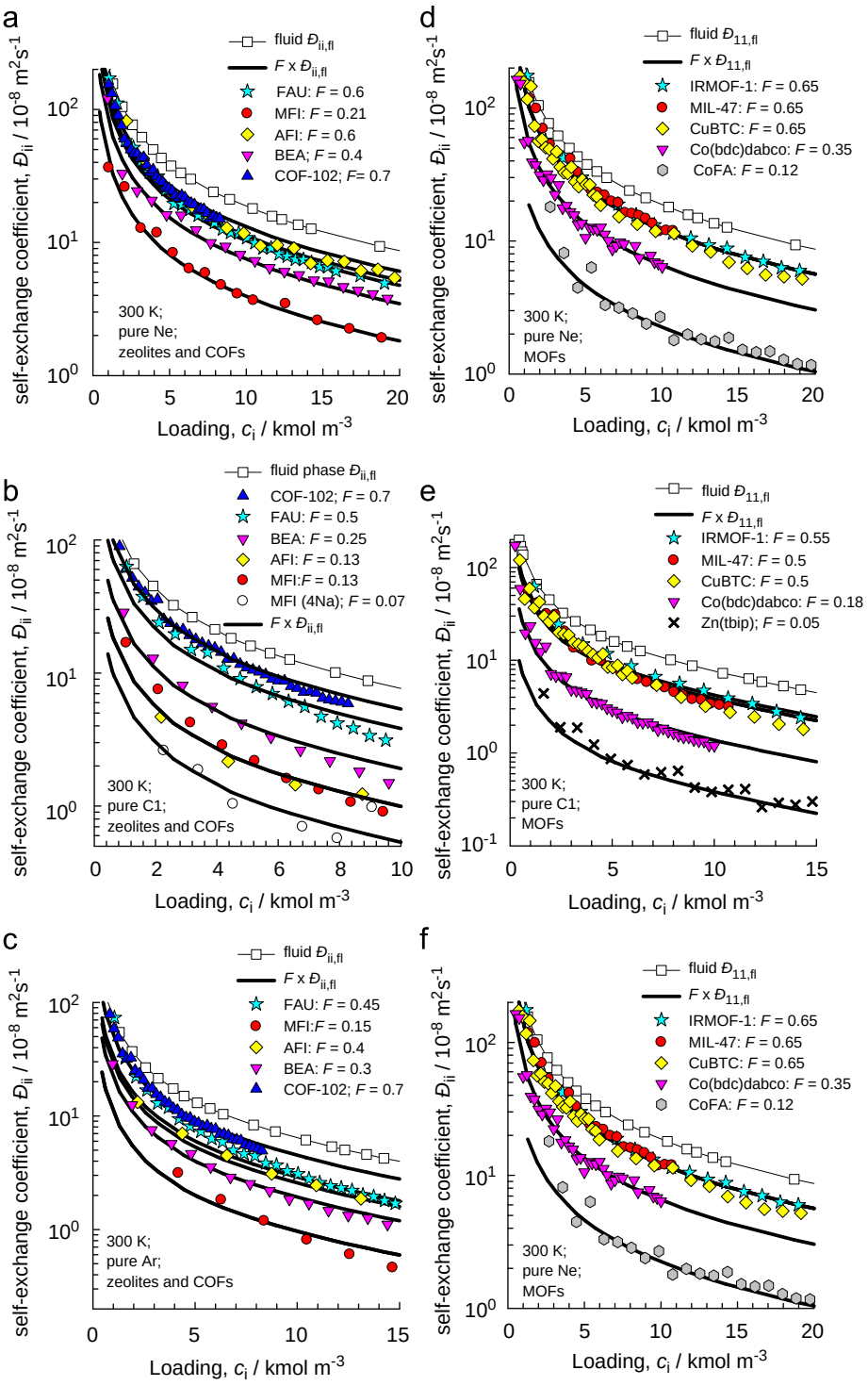

Fig. 12. The self-exchange coefficients $Đ_{ii}$, for diffusion of pure Ne, pure C1, and pure Ar in zeolites, COFs, and MOFs at 300 K as a function of the concentration, c_1. The self-diffusivity in the fluid phase, $Đ_{11,fl}$, obtained from independent MD simulations, are also presented in square symbols, along with continuous solid lines that represent the fraction F_i times $Đ_{ii,fl}$. Note that only a selection of the simulation results are presented here; the complete set of results are available in the supplementary material.

An alternative to the Darken interpolation formula (16) for fluid mixture diffusion is the logarithmic interpolation procedure due to Vignes (1966)

$$Đ_{12,fl} = (Đ_{11,fl})^{x_1}(Đ_{22,fl})^{x_2} \tag{17}$$

This formula is also in good agreement with experimental data, as witnessed in Fig. 14.

Multiplying $Đ_{12,fl}$ with the value of F, taken from the data in Fig. 7a yields an engineering estimate for $Đ_{12}$. Dedicated MD mixture simulations may be needed to getter better estimates of F for use

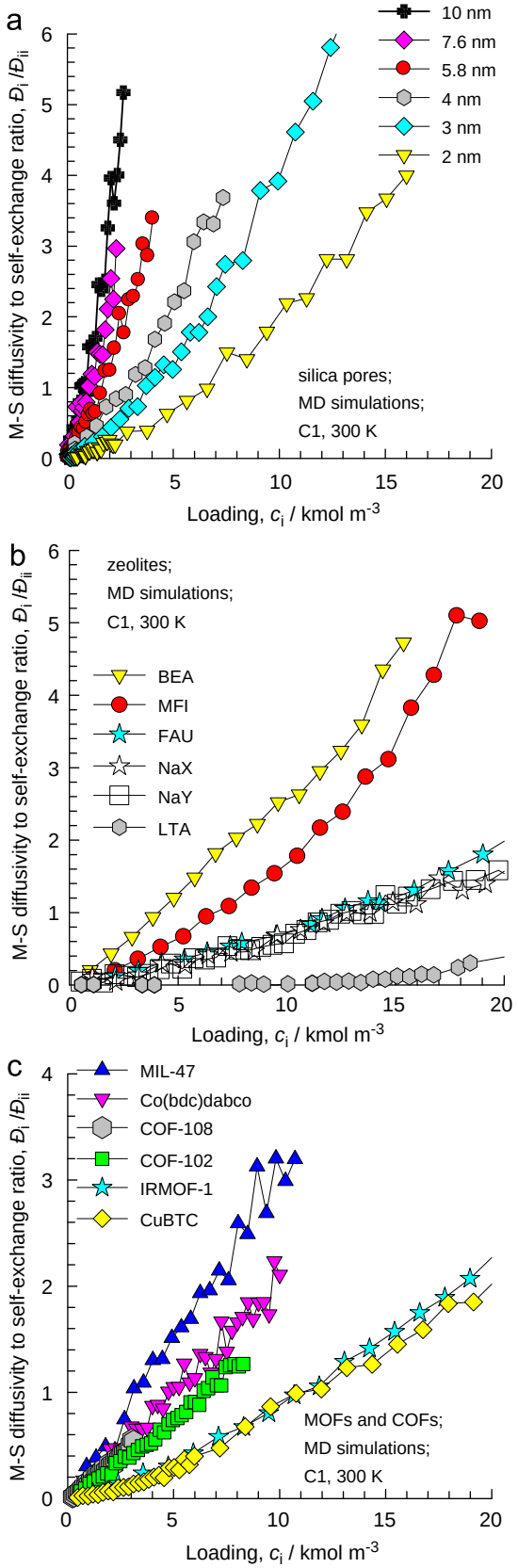

Fig. 13. Ratio of the M–S diffusivity $Đ_i$ with respect to self-exchange coefficient $Đ_{ii}$ for (a) cylindrical pores with $d_p = 2$, 3, 4, 5.8, 7.6, and 10 nm, (b) zeolites (BEA, MFI, FAU, NaX, NaY, LTA), and (c) MOFs (MIL-47, CuBTC, Zn(bdc)dabco, and IRMOF-1), and COF-102.

in engineering design. Another approach is to determine the F_i from MD simulations of unary diffusion for each of the constituent species, and estimate the required value of F for the mixture using a Darken-type interpolation formula

$$F = x_1 F_1 + x_2 F_2 \tag{18}$$

or a Vignes-type interpolation scheme

$$F = (F_1)^{x_1} (F_2)^{x_2} \tag{19}$$

The exchange coefficient in micro-porous materials $Đ_{12}$ can also estimated from information on the self-exchange coefficients $Đ_{ii}$ of the constituent species for the specific guest–host combination using an interpolation formula analogous to Eq. (16)

$$Đ_{12} = x_1 Đ_{11} + x_2 Đ_{22} \tag{20}$$

The accuracy of Eq. (20) is tested in Fig. 15c for diffusion of Ne–Ar, C1–C2, and C1–C3 mixtures in a variety of zeolites and MOFs.

Adopting the Vignes formula for micro-pore diffusion gives

$$Đ_{12} = (Đ_{11})^{x_1} (Đ_{22})^{x_2} \tag{21}$$

As seen in Fig. 15, the calculations following Eq. (21) provides a good estimation of the $Đ_{12}$ in mixtures. Both the Darken and Vignes interpolation formulae are to be preferred to the "empirical" interpolation formula (7), because their more transparent physical basis. Furthermore, they have the distinct advantage that the saturation capacities are not required. The use of Eqs. (20) and (21) requires data on the self-diffusivity, $D_{i,self}$ and M–S diffusivity $Đ_i$ for the constituent species; such information is available only from simulations and not from experiments; these drawbacks also hold for the application of Eq. (7). Generally speaking, Eq. (21) is superior in its predictions when compared to Eq. (20), especially at high loadings c_t; see Fig. 15.

7. Self-diffusivities in *n*-component mixtures

The M–S equations (1) can be applied to derive the following expression for the self-diffusivities in n-component mixtures inside micro- or meso-pores:

$$\frac{1}{D_{i,self}} = \frac{1}{Đ_i} + \sum_{j=1}^{n} \frac{x_j}{Đ_{ij}} = \frac{1}{Đ_i} + \frac{x_i}{Đ_{ii}} + \sum_{\substack{j=1 \\ j\neq i}}^{n} \frac{x_j}{Đ_{ij}}; \quad i = 1, 2, \ldots, n \tag{22}$$

Invoking the Darken or Vignes interpolation schemes, allows the estimation of the $D_{i,self}$ from unary diffusion data. Fig. 16 presents a comparison of MD simulated values of the self-diffusivities $D_{i,self}$ in a variety of a binary mixtures in different micro-porous hosts with the predictions of Eq. (22), along with the Vignes interpolation formula (21). The good predictive capability of the M–S model holds for all the guest–host combinations, as evidenced in the detailed comparisons presented in the Supplementary material.

The expression (22) is useful for the interpretation of experimental NMR data on self diffusivities (Zhao and Snurr, 2009).

8. Estimation of the matrix [Δ] for binary mixture diffusion

For binary mixtures the M–S equations (1) can re-written to evaluate the fluxes N_i explicitly

$$N_i = -\sum_{j=1}^{2} \Delta_{ij} \frac{c_j}{RT} \nabla \mu_j; \quad i = 1, 2 \tag{23}$$

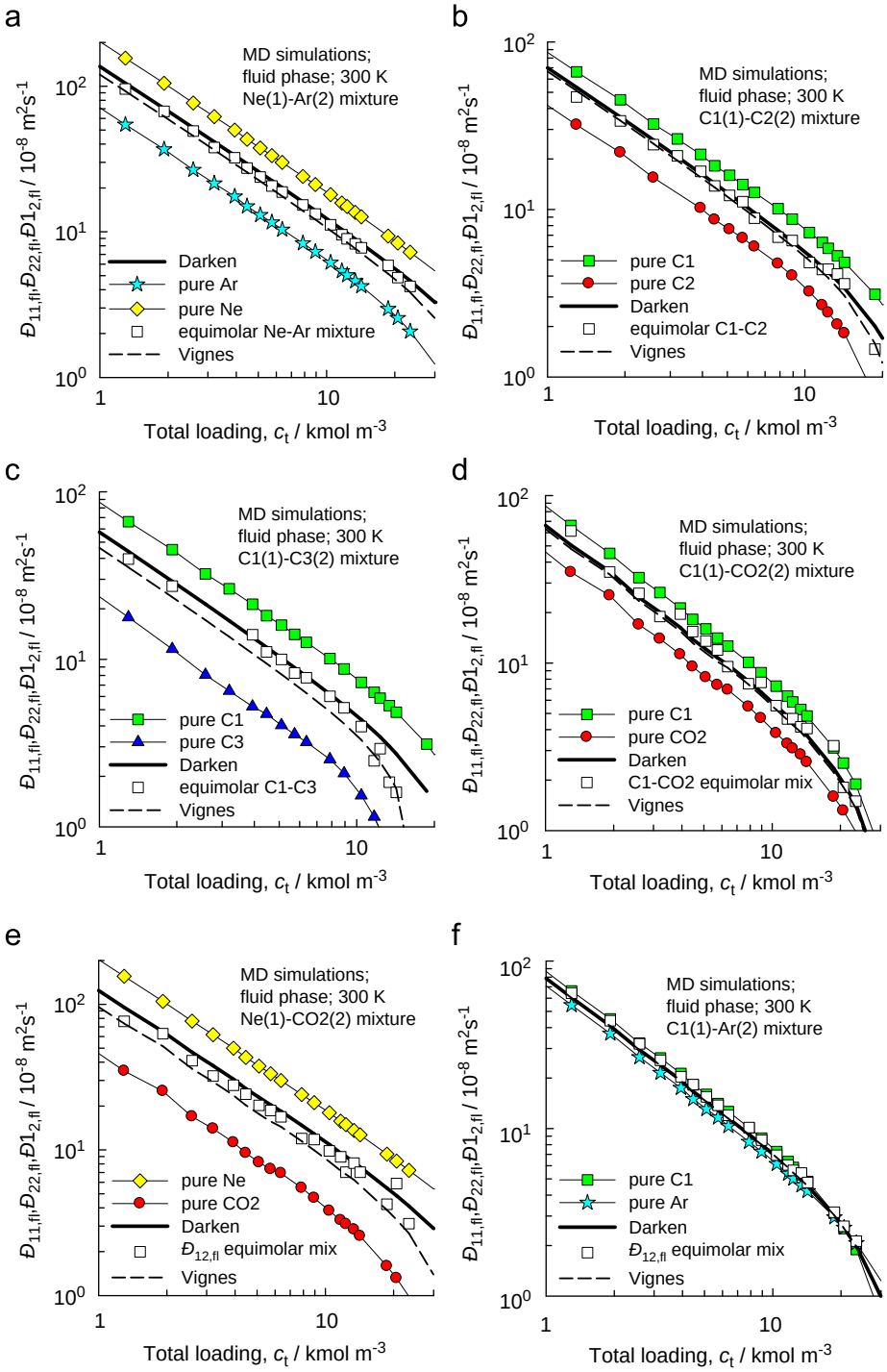

Fig. 14. MD simulations of self-diffusivities, $Đ_{ii,fl}$, along with the $Đ_{12,fl}$ for diffusion in a variety of equimolar binary fluid mixtures as a function of the total fluids concentration, c_t. The calculations of $Đ_{12,fl}$ following Eqs. (16) and (17) are shown by the continuous solid, and dashed lines.

where the elements of Δ_{ij} of the matrix $[\Delta]$ are directly accessible from MD simulations. From Eq. (1) we derive

$$[\Delta] = \begin{bmatrix} \frac{1}{Đ_1} + \frac{x_2}{Đ_{12}} & -\frac{x_1}{Đ_{12}} \\ -\frac{x_2}{Đ_{12}} & \frac{1}{Đ_2} + \frac{x_1}{Đ_{12}} \end{bmatrix}^{-1} \tag{24}$$

Some representative comparisons of the MD simulated values of Δ_{ij} with estimations using MD simulated *unary* diffusion data on $Đ_i$ and $Đ_{ii}$ at the mixture loading c_t, along with the Vignes interpolation formula (21) are shown in Fig. 17. The agreement between the two sets is good for all the guest–host combinations investigated; see information in the Supplementary material.

9. Conclusions

The M–S equations (1) provide an unified description of mixture diffusion in both micro- and meso-porous materials. The unified

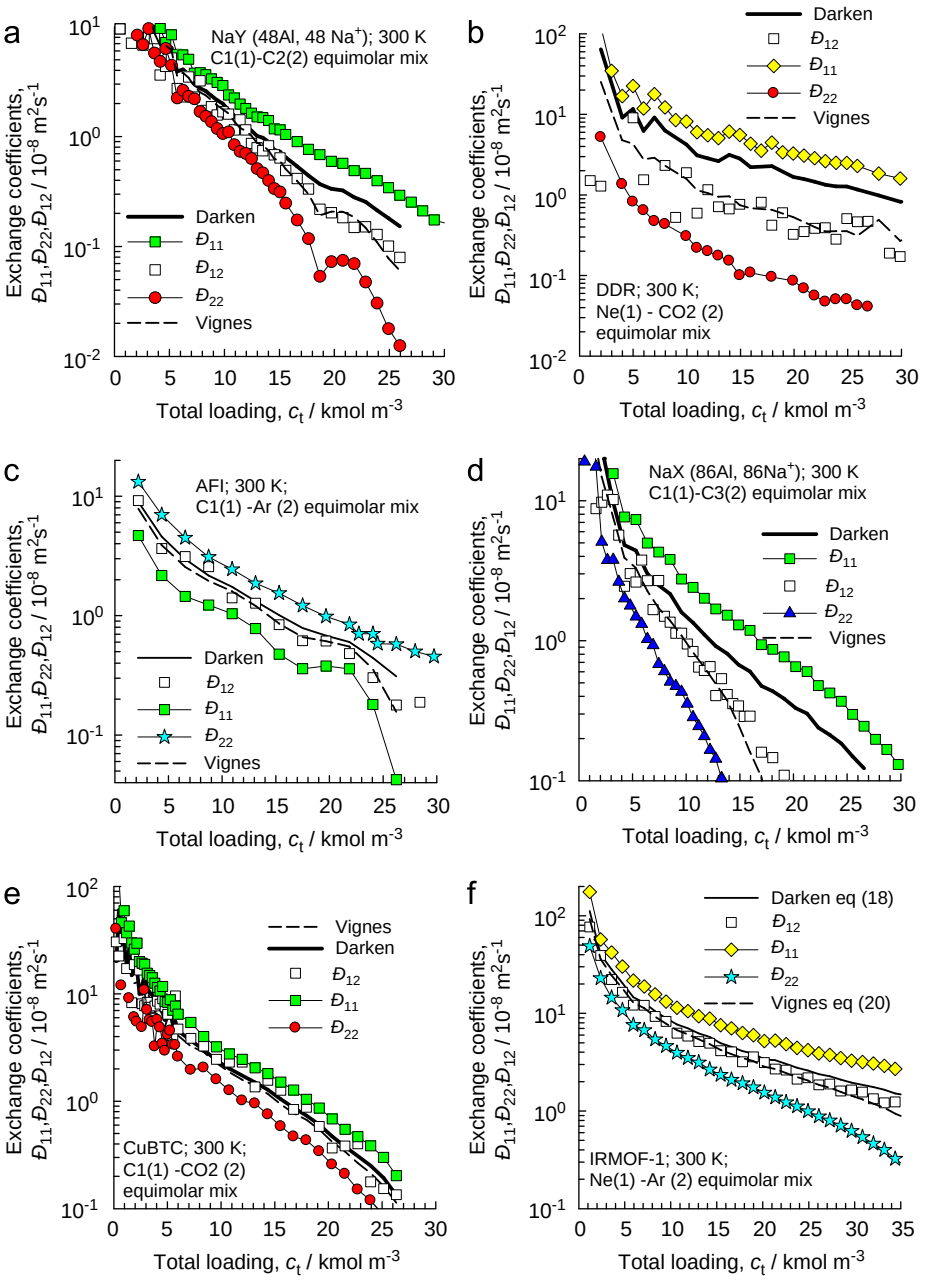

Fig. 15. Test of the Darken equation (20), and Vignes equation (21) for diffusion in a variety of binary mixtures in different micro-porous hosts. A more extensive set of comparisons is to be found in the Supplementary material.

approach uses loadings c_i, expressed in terms of accessible pore volume inside the porous structures.

The major conclusions of the present study are summarized below.

(1) For mixture diffusion inside cylindrical silica meso-pores, $d_p > 2$ nm, the binary exchange coefficient $Đ_{12}$, is found to be equal to the corresponding value in the binary fluid mixture, $Đ_{12,fl}$, over the entire range of mixture concentrations, c_t.
(2) For mixture diffusion inside zeolites, MOFs, and COFs, with channel dimensions smaller than 2 nm, $Đ_{12}$ is found to be lower than $Đ_{12,fl}$, by a constant factor F.
(3) Analogously, the self-exchange coefficient for unary diffusion $Đ_{ii}$ inside micro-porous structures is related to the fluid phase self-diffusivity $Đ_{ii,fl}$ by a constant factor F_i.
(4) Both factors F and F_i show similar dependences on the degree of confinement of guest molecules within the channels of zeolites, MOFs, and COFs; see Fig. 7. Cage-type zeolites with narrow windows, such as CHA, DDR, and LTA, exhibit "rogue" behavior; for these structures the use of uncoupled equations (1), ignoring the first member on the right hand side, is a reasonable approximation for engineering design.
(5) The M–S diffusivity $Đ_i$ for micro-pores has different characteristics than for meso-pores. The $Đ_i - c_i$ dependences are fundamentally different. Other differences have been underlined in the text.
(6) With loadings expressed in terms of the accessible pore volumes, the saturation capacities for a given guest species is approximately the same in various micro-porous host structures; this makes the estimation of $c_{i,sat}$, required in the modeling of

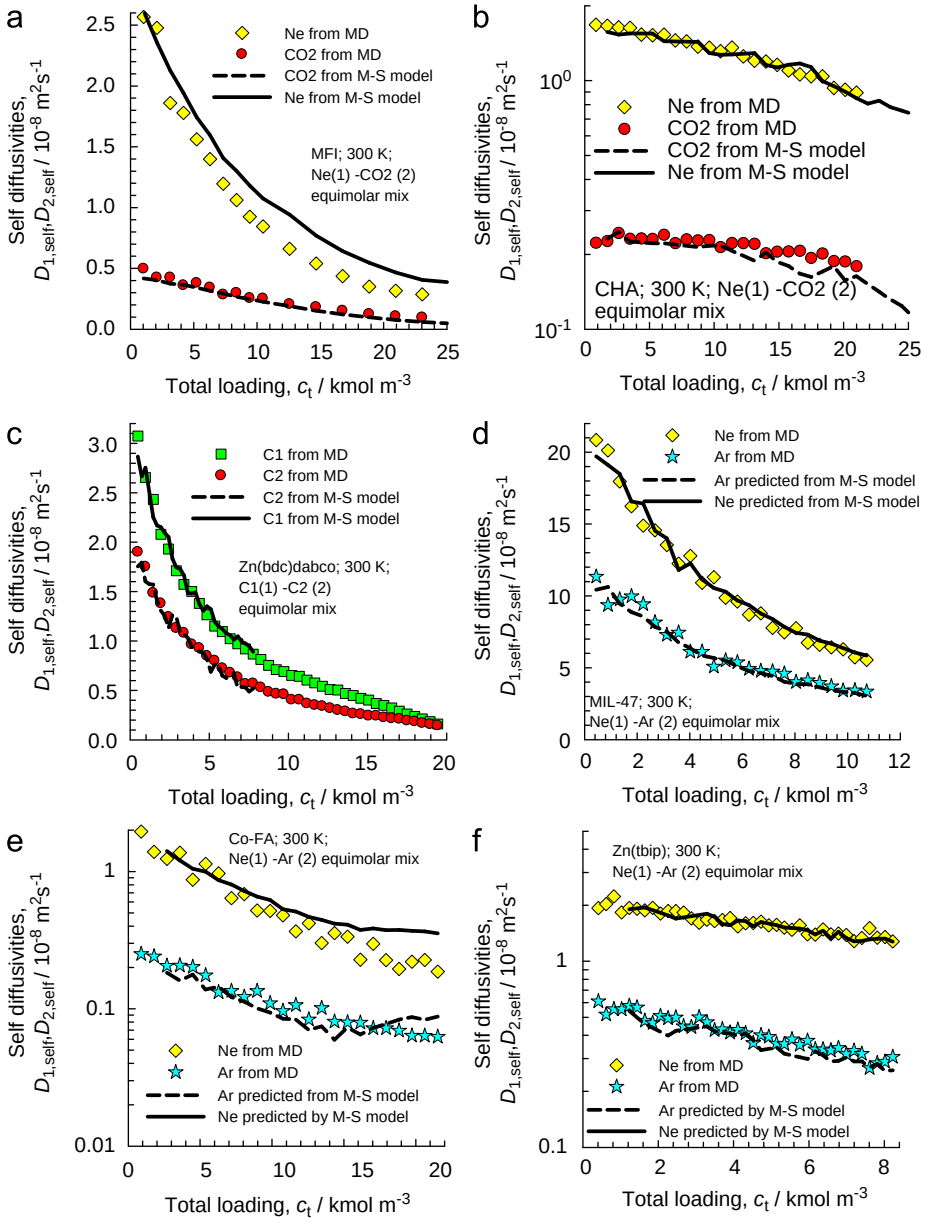

Fig. 16. Comparison of MD simulated values of the self-diffusivities $D_{i,self}$ in a variety of binary mixtures in different micro-porous hosts with the predictions of equation (22), along with the Vignes interpolation formula (21). A more extensive set of comparisons is to be found in the Supplementary material.

the loading dependence of the $Đ_i$, a more tractable proposition.

(7) Correlation effects, as quantified by the ratio $Đ_i/Đ_{ii}$, are stronger in meso-porous than in micro-porous structures. For zeolites, MOFs and COFs, the strength of correlations generally decrease in the following order: (1) 1D and intersecting channels, (2) cavities with wide windows, and (3) cages separated by narrow windows.

(8) Either the Darken-type equation (20) or the Vignes-type equation (21) are to be preferred to the "empirical" interpolation formula (7) because of their more transparent physical basis. These equations allow estimation of the $Đ_{12}$ for mixture diffusion from the unary self exchange $Đ_{ii}$. The extensive tests presented in the Supplementary material indicate the Vignes equation (21) to be the preferred interpolation scheme and is recommended for use.

(9) Multiplying the F, estimated using data in Fig. 7 or from dedicated MD simulations, with the fluid phase $Đ_{12,fl}$ provides an engineering estimate for the $Đ_{12}$.

(10) The unified description seamlessly bridges the values of the exchange coefficient $Đ_{12}$ for micro- and meso-porous materials as a function of the degree of confinement.

The unified approach to modeling of diffusion in micro- and meso-porous materials is particularly convenient for use in engineering design of separation and reaction systems using hybrid materials, such as biporous adsorbents (Delgado and Rodrigues, 2001), meso-porous zeolites (Hoang et al., 2005) and mixed matrix membranes (Sheffel and Tsapatsis, 2009).

Notation

c_i	concentration of species i, mol m^{-3}
c_t	total concentration in mixture, mol m^{-3}

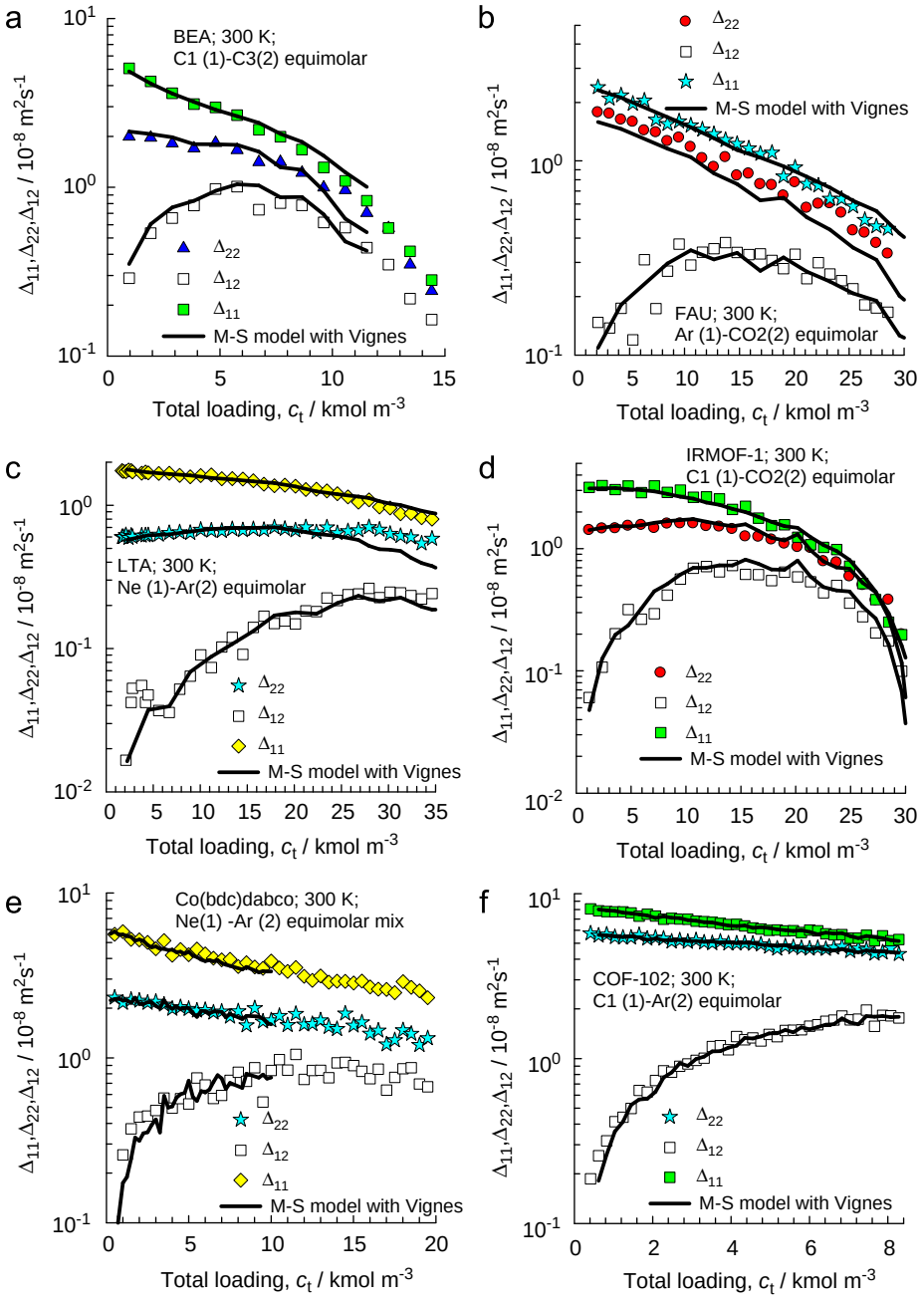

Fig. 17. Comparison of MD simulated values of Δ_{ij} in a variety of binary mixtures in different micro-porous hosts with the predictions of Eq. (24), along with the Vignes interpolation formula (21). A more extensive set of comparisons is to be found in the Supplementary material.

d_p	pore diameter, m
$D_{i,self}$	self-diffusivity of species i within pore, m^2 s^{-1}
$Đ_{ii}$	self-exchange coefficient, m^2 s^{-1}
$Đ_{ii,fl}$	self-diffusivity of species i in fluid phase, m^2 s^{-1}
$Đ_i$	M–S diffusivity for molecule–wall interaction, m^2 s^{-1}
$Đ_i(0)$	zero-loading M–S diffusivity for molecule–wall interaction, m^2 s^{-1}
$Đ_{12}$	M–S exchange coefficient defined by Eq. (1), m^2 s^{-1}
$Đ^*_{12}$	M–S exchange coefficient defined by Eq. (4), m^2 s^{-1}
$Đ_{12,fl}$	M–S diffusivity in binary fluid mixture, m^2 s^{-1}
$D_{i,Kn}$	Knudsen diffusivity of species i, m^2 s^{-1}
f_i	bulk fluid phase fugacity of species i, Pa
F	factor defined by Eq. (9), dimensionless
F_i	factor defined by Eq. (15), dimensionless
k_B	Boltzmann constant, 1.38×10^{-23} J molecule^{-1} K^{-1}
n	number of components in mixture, dimensionless
N_i	molar flux of species i, mol m^{-2} s^{-1}
R	gas constant, 8.314 J mol^{-1} K^{-1}
T	absolute temperature, K
x_i	mole fraction of species i based on loading within pore, dimensionless

Greek letters

Δ_{ij}	diffusivities defined by Eq. (23), m^2 s^{-1}
ε	Lennard-Jones interaction energy parameter, J molecule^{-1}

η_i	viscosity of species i, Pa s
θ_i	fractional occupancy of species i, dimensionless
μ_i	molar chemical potential, J mol^{-1}
ρ	framework density, kg m^{-3}
σ	Lennard-Jones size parameter, m
ϕ	fractional pore volume, dimensionless

Subscripts

fl	referring to fluid phase
i	referring to component *i*
t	referring to total mixture
Kn	referring to Knudsen

Acknowledgment

RK acknowledges the grant of a TOP subsidy from the Netherlands Foundation for Fundamental Research (NWO-CW) for intensification of reactors.

Appendix A. Supplementary material

Supplementary data associated with this article can be found in the online version at doi:10.1016/j.ces.2009.03.047.

References

Alaerts, L., Kirschhock, C.E.A., Maes, M., van der Veen, M., Finsy, V., Depla, A., Martens, J.A., Baron, G.V., Jacobs, P.A., Denayer, J.F.M., De Vos, D., 2007. Selective adsorption and separation of xylene isomers and ethylbenzene with the microporous vanadium(IV) terephthalate MIL-47. Angewandte Chemie—International Edition 46, 4293–4297.

Amirjalayer, S., Tafipolsky, M., Schmid, R., 2007. Molecular dynamics simulation of benzene diffusion in MOF-5: importance of lattice dynamics. Angewandte Chemie—International Edition 46, 463–466.

Bárcia, P.S., Zapata, F., Silva, J.A.C., Rodrigues, A.E., Chen, B., 2008. Kinetic separation of hexane isomers by fixed-bed adsorption with a microporous metal–organic framework. Journal of Physical Chemistry B 111, 6101–6103.

Barrer, R.M., Sutherland, J.W., 1956. Inclusion complexes of faujasite with paraffins and permanent gases. Proceedings of the Royal Society of London Series A 237, 439–463.

Barthelet, K., Marrot, J., Riou, D., Férey, G., 2007. A breathing hybrid organic-inorganic solid with very large pores and high magnetic characteristics. Angewandte Chemie—International Edition 41, 281–284.

Beerdsen, E., Dubbeldam, D., Smit, B., 2005. Molecular understanding of diffusion in confinement. Physical Review Letters 95, 164505.

Beerdsen, E., Dubbeldam, D., Smit, B., 2006. Understanding diffusion in nanoporous materials. Physical Review Letters 96, 044501.

Bhatia, S.K., Nicholson, D., 2003. Molecular transport in nanopores. Journal of Chemical Physics 119, 1719–1730.

Bidlack, D.L., Anderson, D.K., 1964. Mutual diffusion in the system hexane–hexadecane. Journal of Physical Chemistry 68, 206–208.

Chempath, S., Krishna, R., Snurr, R.Q., 2004. Nonequilibrium MD simulations of diffusion of binary mixtures containing short *n*-alkanes in faujasite. Journal of Physical Chemistry B 108, 13481–13491.

Chmelik, C., Heinke, L., Kärger, J., Shah, D.B., Schmidt, W., van Baten, J.M., Krishna, R., 2008. Inflection in the loading dependence of the Maxwell–Stefan diffusivity of iso-butane in MFI zeolite. Chemical Physics Letters 459, 141–145.

Chmelik, C., Kärger, J., Wiebcke, M., Caro, J., van Baten, J.M., Krishna, R., 2009. Adsorption and diffusion of alkanes in CuBTC crystals investigated using infrared microscopy and molecular simulations. Microporous and Mesoporous Materials 117, 22–32.

Chui, S.S.Y., Lo, S.M.F., Charmant, J.P.H., Orpen, A.G., Williams, I.D., 1999. A chemically functionalizable nanoporous material $[Cu_3(TMA)_2(H2O)_3]_n$. Science 283, 1148–1150.

Czaja, A.U., Trukhan, N., Müller, U., 2009. Industrial applications of metal–organic frameworks. Chemical Society Reviews, in press ⟨http://dx.doi.org/10.1039/b804680h⟩.

Darken, L.S., 1948. Diffusion, mobility and their interrelation through free energy in binary metallic systems. Transactions of the American Institute of Mining and Metallurgical Engineers 175, 184–201.

Delgado, J.A., Rodrigues, A.E., 2001. A Maxwell–Stefan model of bidisperse pore pressurization for Langmuir adsorption of gas mixtures. Industrial & Engineering Chemistry Research 40, 2289–2301.

Dubbeldam, D., Calero, S., Maesen, T.L.M., Smit, B., 2003. Understanding the window effect in zeolite catalysis. Angewandte Chemie—International Edition 42, 3624–3626.

Dubbeldam, D., Frost, H., Walton, K.S., Snurr, R.Q., 2007a. Molecular simulation of adsorption sites of light gases in the metal–organic framework IRMOF-1. Fluid Phase Equilibria 261, 152–161.

Dubbeldam, D., Galvin, C.J., Walton, K.S., Ellis, D.E., Snurr, R.Q., 2008. Separation and molecular-level segregation of complex alkane mixtures in metal–organic frameworks. Journal of the American Chemical Society 130, 10884–10885.

Dubbeldam, D., Smit, B., 2003. Computer simulation of incommensurate diffusion in zeolites: Understanding window effects. Journal of Physical Chemistry B 107, 12138–12152.

Dubbeldam, D., Walton, K.S., Ellis, D.E., Snurr, R.Q., 2007b. Exceptional negative thermal expansion in isoreticular metal–organic frameworks. Angewandte Chemie—International Edition 46, 4496–4499.

Dybtsev, D.N., Chun, H., Yoon, S.H., Kim, D., Kim, K., 2004. Microporous manganese formate: a simple metal–organic porous material with high framework stability and highly selective gas sorption properties. Journal of the American Chemical Society 126, 32–33.

Dysthe, D.K., Fuchs, A.H., Rousseau, B., Durandeau, M., 1999. Fluid transport properties by equilibrium molecular dynamics. II. Multicomponent systems. Journal of Chemical Physics 110, 4060–4067.

El-Kaderi, H.M., Hunt, J.R., Mendoza-Cortés, J.L., Côté, A.P., Taylor, R.E., O'Keeffe, M., Yaghi, O.M., 2007. Designed synthesis of 3D covalent organic frameworks. Science 316, 268–272.

Farooq, S., Ruthven, D.M., 1991. Numerical-simulation of a kinetically controlled pressure swing adsorption bulk separation process based on a diffusion-model. Chemical Engineering Science 46, 2213–2224.

Férey, G., 2008. Hybrid porous solids: past, present, future. Chemical Society Reviews 37, 191–214.

Fernández, G.A., Vrabec, J., Hasse, H., 2004. Self diffusion and binary Maxwell–Stefan diffusion in simple fluids with the Green–Kubo method. International Journal of Thermophysics 25, 175–186.

Finsy, V., Verelst, H., Alaerts, L., De Vos, D., Jacobs, P.A., Baron, G.V., Denayer, J.F.M., 2008. Pore-filling-dependent selectivity effects in the vapor-phase separation of xylene isomers on the metal–organic framework MIL-47. Journal of the American Chemical Society 130, 7110–7118.

Frenkel, D., Smit, B., 2002. Understanding Molecular Simulations: From Algorithms to Applications. second ed. Academic Press, San Diego.

Fritzsche, S., Haberlandt, R., Kärger, J., Pfeifer, H., Heinzinger, K., Wolfsberg, M., 1995. Influence of exchangeable cations on the diffusion of neutral diffusants in zeolites of type LTA-an MD study. Chemical Physics Letters 242, 361–366.

Gavalas, G.R., 2008. Diffusion in microporous membranes: measurements and modeling. Industrial & Engineering Chemistry Research 47, 5797–5811.

Golden, T.C., Sircar, S., 1994. Gas adsorption on silicalite. Journal of Colloid and Interface Science 162, 182–188.

Goo, G.H., Sung, G.H., Lee, S.H., Chang, T.Y., 2002. Diffusion behavior of *n*-alkanes by molecular dynamics simulations. Bulletin of the Korean Chemical Society 23, 1595–1603.

Greathouse, J.A., Allendorf, M.D., 2008. Force field validation for molecular dynamics simulations of IRMOF-1 and other isoreticular zinc carboxylate coordination polymers. Journal of Physical Chemistry C 112, 5795–5802.

Habgood, H.W., 1958. The kinetics of molecular sieve action. Sorption of nitrogen–methane mixtures by Linde molecular sieve 4A. Canadian Journal of Chemistry 36, 1384–1397.

Hansen, N., Krishna, R., van Baten, J.M., Bell, A.T., Keil, F.J., 2009. Analysis of diffusion limitation in the alkylation of benzene over H-ZSM-5 by combining quantum chemical calculations, molecular simulations, and a continuum approach. Journal of Physical Chemistry C 113, 235–246.

Hedin, N., DeMartin, G.J., Roth, W.J., Strohmaier, K.G., Reyes, S.C., 2008. PFG NMR self-diffusion of small hydrocarbons in high silica DDR, CHA and LTA structures. Microporous and Mesoporous Materials 109, 327–334.

Hedin, N., DeMartin, G.J., Strohmaier, K.G., Reyes, S.C., 2007. PFG NMR self-diffusion of propylene in ITQ-29, CaA and NaCaA: window size and cation effects. Microporous and Mesoporous Materials 98, 182–188.

Heinke, L., Tzoulaki, D., Chmelik, C., Hibbe, F., van Baten, J.M., Lim, H., Li, J., Krishna, R., Kärger, J., 2009. Assessing guest diffusivities in porous hosts from transient concentration profiles. Physical Review Letters 102, 065901.

Helbaek, M., Hafskjold, B., Dysthe, D.K., Sorland, G.H., 1996. Self-diffusion coefficients of methane or ethane mixtures with hydrocarbons at high pressure by NMR. Journal of Chemical and Engineering Data 41, 598–603.

Higgins, S., DeSisto, W., Ruthven, D.M., 2009. Diffusive transport through mesoporous silica membranes. Microporous and Mesoporous Materials 117, 268–277.

Hoang, V.T., Huang, Q., Malekian, A., Eic, M., Do, T.O., Kaliaguine, S., 2005. Diffusion characterization of a novel mesoporous zeolitic material. Adsorption—Journal of the International Adsorption Society 11, 421–426.

Jobic, H., Laloué, C., Laroche, C., van Baten, J.M., Krishna, R., 2006. Influence of isotherm inflection on the loading dependence of the diffusivities of *n*-hexane and *n*-heptane in MFI zeolite. Quasi-elastic neutron scattering experiments supplemented by molecular simulations. Journal of Physical Chemistry B 110, 2195–2201.

Jobic, H., Methivier, A., Ehlers, G., Farago, B., Haeussler, W., 2004. Accelerated diffusion of long-chain alkanes between nanosized cavities. Angewandte Chemie—International Edition 43, 364–366.

Kärger, J., Ruthven, D.M., 1992. Diffusion in Zeolites and Other Microporous Solids. Wiley, New York.

Kerkhof, P.J.A.M., 1996. A modified Maxwell–Stefan model for transport through inert membranes: the binary friction model. Chemical Engineering Journal 64, 319–343.

Keskin, S., Liu, J., Rankin, R.B., Johnson, J.K., Sholl, D.S., 2009. Progress, opportunities, and challenges for applying atomically detailed modeling to molecular adsorption and transport in metal–organic framework materials. Industrial & Engineering Chemistry Research 48, 2355–2371.

Krishna, R., 1990. Multicomponent surface diffusion of adsorbed species—a description based on the generalized Maxwell–Stefan equations. Chemical Engineering Science 45, 1779–1791.

Krishna, R., Li, S., van Baten, J.M., Falconer, J.L., Noble, R.D., 2008. Investigation of slowing-down and speeding-up effects in binary mixture permeation across SAPO-34 and MFI membranes. Separation and Purification Technology 60, 230–236.

Krishna, R., van Baten, J.M., 2005a. The Darken relation for multicomponent diffusion in liquid mixtures of linear alkanes. An investigation using molecular dynamics (MD) simulations. Industrial & Engineering Chemistry Research 44, 6939–6947.

Krishna, R., van Baten, J.M., 2005b. Diffusion of alkane mixtures in zeolites. Validating the Maxwell–Stefan formulation using MD simulations. Journal of Physical Chemistry B 109, 6386–6396.

Krishna, R., van Baten, J.M., 2006. Describing binary mixture diffusion in carbon nanotubes with the Maxwell–Stefan equations. An investigation using molecular dynamics simulations. Industrial & Engineering Chemistry Research 45, 2084–2093.

Krishna, R., van Baten, J.M., 2008a. Onsager coefficients for binary mixture diffusion in nanopores. Chemical Engineering Science 63, 3120–3140.

Krishna, R., van Baten, J.M., 2008b. Insights into diffusion of gases in zeolites gained from molecular dynamics simulations. Microporous and Mesoporous Materials 109, 91–108.

Krishna, R., van Baten, J.M., 2008c. Segregation effects in adsorption of CO_2 containing mixtures and their consequences for separation selectivities in cage-type zeolites. Separation and Purification Technology 61, 414–423.

Krishna, R., van Baten, J.M., 2009a. An investigation of the characteristics of Maxwell–Stefan diffusivities of binary mixtures in silica nanopores. Chemical Engineering Science 64, 870–882.

Krishna, R., van Baten, J.M., 2009b. A molecular dynamics investigation of a variety of influences of temperature on diffusion in zeolites. Microporous and Mesoporous Materials, in press ⟨http://dx.doi.org/10.1016/j.micromeso.2009.01.015⟩.

Krishna, R., van Baten, J.M., 2009c. A molecular simulation study of commensurate—incommensurate adsorption of *n*-alkanes in cobalt formate frameworks. Molecular Simulation, in press ⟨http://dx.doi.org/10.1080/08927020902744672⟩.

Krishna, R., van Baten, J.M., García-Pérez, E., Calero, S., 2007. Incorporating the loading dependence of the Maxwell–Stefan diffusivity in the modeling of CH_4 and CO_2 permeation across zeolite membranes. Industrial & Engineering Chemistry Research 46, 2974–2986.

Lee, J.Y., Olson, D.H., Pan, L., Emge, T.J., Li, J., 2007. Microporous metal–organic frameworks with high gas sorption and separation capacity. Advanced Functional Materials 17, 1255–1262.

Li, K., Olson, D.H., Lee, J.Y., Bi, W., Wu, K., Yuen, T., Xu, Q., Li, J., 2008. Multifunctional microporous MOFs exhibiting gas/hydrocarbon adsorption selectivity, separation capability and three-dimensional magnetic ordering. Advanced Functional Materials 18, 2205–2214.

Li, S., Falconer, J.L., Noble, R.D., Krishna, R., 2007a. Modeling permeation of CO_2/CH_4, CO_2/N_2, and N_2/CH_4 mixtures across SAPO-34 membrane with the Maxwell–Stefan equations. Industrial & Engineering Chemistry Research 46, 3904–3911.

Li, S., Falconer, J.L., Noble, R.D., Krishna, R., 2007b. Interpreting unary, binary and ternary mixture permeation across a SAPO-34 membrane with loading-dependent Maxwell–Stefan diffusivities. Journal of Physical Chemistry C 111, 5075–5082.

Mason, E.A., Malinauskas, A.P., 1983. Gas Transport in Porous Media: The Dusty-Gas Model. Elsevier, Amsterdam.

Merzliak, T., Pfennig, A., 2004. Development of a model for the description of intra-diffusion in homogeneous liquid Lennard-Jones mixtures. Molecular Simulation 30, 459–468.

Myers, A.L., Monson, P.A., 2002. Adsorption in porous materials at high pressure: theory and experiment. Langmuir 18, 10261–10273.

Naumov, S., Valiullin, V., Galvosas, P., Kärger, J., Monson, P.A., 2007. Diffusion hysteresis in mesoporous materials. The European Physical Journal—Special Topics 141, 107–112.

Pan, L., Olson, D.H., Ciemnolonski, L.R., Heddy, R., Li, J., 2006a. Separation of hydrocarbons with a microporous metal–organic framework. Angewandte Chemie—International Edition 45, 616–619.

Pan, L., Parker, B., Huang, X., Olson, D.H., Lee, J.Y., Li, J., 2006b. Zn(tbip) (H_2 tbip) = 5-*tert*-Butyl Isophthalic Acid): a highly stable guest-free microporous metal organic framework with unique gas separation capability. Journal of the American Chemical Society 128, 4180–4181.

Poling, B.E., Prausnitz, J.M., O'Connell, J.P., 2001. The Properties of Gases and Liquids. fifth ed. McGraw-Hill, New York.

Reed, D.A., Ehrlich, G., 1981. Surface diffusion, atomic jump rates and thermodynamics. Surface Science 102, 588–609.

Ruthven, D.M., 1984. Principles of Adsorption and Adsorption Processes. Wiley, New York.

Seehamart, K., Nanok, T., Krishna, R., van Baten, J.M., Remsungnen, T., Fritzsche, S., 2009. A molecular dynamics investigation of the influence of framework flexibility on self-diffusivity of ethane in Zn(tbip) frameworks. Microporous and Mesoporous Materials, in press ⟨http://dx.doi.org/10.1016/j.micromeso.2009.01.020⟩.

Sheffel, J.A., Tsapatsis, M., 2009. A semi-empirical approach for predicting the performance of mixed matrix membranes containing selective flakes. Journal of Membrane Science 326, 595–607.

Shieh, J.C., Lyons, P.A., 1969. Transport properties of liquid *n*-alkanes. Journal of Physical Chemistry 73, 3258–3264.

Skoulidas, A.I., Sholl, D.S., Krishna, R., 2003. Correlation effects in diffusion of CH_4/CF_4 mixtures in MFI zeolite. A study linking MD simulations with the Maxwell–Stefan formulation. Langmuir 19, 7977–7988.

Talu, O., Myers, A.L., 2001. Molecular simulation of adsorption: Gibbs dividing surface and comparison with experiment. American Institute of Chemical Engineers Journal 47, 1160–1168.

Tzoulaki, D., Heinke, L., Lim, H., Li, J., Olson, D., Caro, J., Krishna, R., Chmelik, C., Kärger, J., 2009. Assessing surface permeabilities from transient guest profiles in nanoporous host materials. Angewandte Chemie—International Edition, in press ⟨http://dx.doi.org/10.1002/anie.200804785⟩.

Valiullin, V., Naumov, S., Galvosas, P., Kärger, J., Woo, H.J., Porcheron, F., Monson, P.A., 2006. Exploration of molecular dynamics during transient sorption of fluids in mesoporous materials. Nature 443, 965–968.

van de Graaf, J.M., Kapteijn, F., Moulijn, J.A., 1999. Modeling permeation of binary mixtures through zeolite membranes. American Institute of Chemical Engineers Journal 45, 497–511.

van den Bergh, J., Zhu, W., Gascon, J., Moulijn, J.A., Kapteijn, F., 2008. Separation and permeation characteristics of a DD3R zeolite membrane. Journal of Membrane Science 316, 35–45.

van den Bergh, J., Zhu, W., Groen, J.C., Kapteijn, F., Moulijn, J.A., Yajima, K., Nakayama, K., Tomita, T., Yoshida, S., 2007. Natural gas purification with a DDR zeolite membrane; permeation modelling with Maxwell–Stefan equations. Studies in Surface Science and Catalysis 170, 1021–1027.

Vignes, A., 1966. Diffusion in binary solutions. Industrial & Engineering Chemistry Fundamentals 5, 189–199.

Wang, H., Getzschmann, J., Senkovska, I., Kaskel, S., 2008. Structural transformation and high pressure methane adsorption of Co_2(1,4-bdc)$_2$dabco. Microporous and Mesoporous Materials 116, 653–657.

Wang, R., Farooq, S., Tien, C., 1999. Maxwell–Stefan theory for macropore molecular-diffusion-controlled fixed-bed adsorption. Chemical Engineering Science 54, 4089–4098.

Wang, Y., LeVan, M.D., 2007. Mixture diffusion in nanoporous adsorbents: development of Fickian flux relationship and concentration-swing frequency response method. Industrial & Engineering Chemistry Research 46, 2141–2154.

Wang, Y., LeVan, M.D., 2008. Mixture diffusion in nanoporous adsorbents: equivalence of Fickian and Maxwell–Stefan approaches. Journal of Physical Chemistry B 112, 8600–8604.

Wheeler, D.R., Newman, J., 2004. Molecular dynamics simulations of multicomponent diffusion. 1. Equilibrium method. Journal of Physical Chemistry B 108, 18353–18361.

Yaghi, O.M., 2007. Metal–organic frameworks: a tale of two entanglements. Nature Materials 6, 92–93.

Yang, Q., Zhong, C., 2006. Electrostatic-field-induced enhancement of gas mixture separation in metal–organic frameworks: a computational study. ChemPhysChem 7, 1417–1421.

Young, J.B., Todd, B., 2005. Modelling of multi-component gas flows in capillaries and porous solids. International Journal of Heat and Mass Transfer 48, 5338–5353.

Yu, Y.X., Gao, G.H., 2000. Lennard-Jones chain model for self-diffusion of *n*-alkanes. International Journal of Thermophysics 21, 57–70.

Zabala, D., Nieto-Draghi, C., de Hemptinne, J.C., López de Ramos, A.L., 2008. Diffusion coefficients in CO_2/*n*-alkane binary liquid mixtures by molecular simulation. Journal of Physical Chemistry B 112, 16610–16618.

Zhao, Q., Snurr, R.Q., 2009. Self-diffusion studies of binary mixtures in NaX zeolites using pulsed field gradient NMR and a Maxwell–Stefan model. Journal of Physical Chemistry A, in press ⟨http://dx.doi.org/10.1021/jp810058z⟩.

Zimmermann, N.E.R., Jakobtorweihen, S., Beerdsen, E., Smit, B., Keil, F.J., 2007. In-depth study of the influence of host-framework flexibility on the diffusion of small gas molecules in one-dimensional zeolitic pore systems. Journal of Physical Chemistry C 111, 17370–17381.